Progressive environmental deterioration in northwestern Pangea leading to the latest Permian extinction

Stephen E. Grasby[1,2,†], Benoit Beauchamp[2], David P.G. Bond[3], Paul Wignall[4], Cristina Talavera[5], Jennifer M. Galloway[1], Karsten Piepjohn[6], Lutz Reinhardt[6], and Dierk Blomeier[7]

[1]*Geological Survey of Canada, Natural Resources Canada, 3303 33rd Street NW, Calgary, Alberta T2L 2A7, Canada*
[2]*Department of Geoscience, University of Calgary, 2500 University Drive NW, Calgary, Alberta T2N 1N4, Canada*
[3]*Department of Geography, Environment and Earth Sciences, University of Hull, Hull HU6 7RX, UK*
[4]*School of Earth Sciences, University of Leeds, Woodhouse Lane, Leeds LS2 9JT, UK*
[5]*Department of Imaging and Applied Physics, Curtin University, Kent Street, Bentley, WA 6102, Australia*
[6]*Bundesanstalt für Geowissenschaften und Rohstoffe, Geozentrum Hannover, Stilleweg 2, D-30655 Hannover, Germany*
[7]*Millennia Stratigraphic Consultants, 35 Swansfield, Lechlade GL7 3SF, UK*

ABSTRACT

Stratigraphic records from northwestern Pangea provide unique insight into global processes that occurred during the latest Permian extinction (LPE). We examined a detailed geochemical record of the Festningen section, Spitsbergen. A stepwise extinction is noted as: starting with (1) loss of carbonate shelly macrofauna, followed by (2) loss of siliceous sponges in conjunction with an abrupt change in ichnofabrics as well as dramatic change in the terrestrial environment, and (3) final loss of all trace fossils. We interpret loss of carbonate producers as related to shoaling of the lysocline in higher latitudes, in relationship to building atmospheric CO_2. The loss of siliceous sponges is coincident with the global LPE event and is related to onset of high loading rates of toxic metals (Hg, As, Co) that we suggest are derived from Siberian Trap eruptions. The final extinction stage is coincident with redox-sensitive trace metal and other proxy data that suggest onset of anoxia after the other extinction events. These results show a remarkable record of progressive environmental deterioration in northwestern Pangea during the extinction crises.

INTRODUCTION

The latest Permian extinction (LPE) represents a period of dramatic climate change associated with disruption of global biogeochemical cycles and the worst mass extinction event in Earth history. Over 90% of marine species and 70% of terrestrial vertebrates went extinct at this time (Erwin, 2006). While numerous extinction mechanisms have been proposed, growing evidence supports environmental effects associated with massive eruption of the Siberian Traps (Campbell et al., 1992; Grasby et al., 2011; Renne et al., 1995; Saunders and Reichow, 2009; Shen et al., 2011; Wignall, 2001). The original volume of the Siberian Traps and West Siberian rift system is difficult to estimate, but upper-end figures of 3–4 × 10^6 km^3 (Courtillot et al., 1999; Fedorenko et al., 2000) make this mega-scale eruption one of the largest in Earth history. Magma intruded through the Tunguska Basin, and was associated with combustion of organic-rich sediments (Grasby et al., 2011; Reichow et al., 2009; Retallack and Jahren, 2008; Retallack and Krull, 2006; Svensen et al., 2009) along with release of large volumes of CO_2 (White and Saunders, 2005; Wignall, 2001), deleterious atmospheric gases (Beerling et al., 2007; Black et al., 2012, 2014; Kaiho and Koga, 2013; Svensen et al., 2009), and toxic elements (Grasby et al., 2011, 2013a; Sanei et al., 2012). Oxygen isotope records suggest that rapid global warming and extremely high ocean temperatures developed at this time (Romano et al., 2013; Sun et al., 2012), invoking a hothouse scenario (Kidder and Worsley, 2010; Retallack, 1999; Song et al., 2014). Acid ocean conditions may also have developed (Beauchamp and Grasby, 2012; Heydari and Hassanzadeh, 2003; Kidder and Worsley, 2004, 2010; Liang, 2002; Payne et al., 2007). Global anoxia has long been suggested to be an important environmental stress associated with the LPE (Isozaki, 1997; Knoll et al., 1996; Wignall and Hallam, 1992; Wignall and Twitchett, 1996). While some regions show evidence of photic zone euxinia in the Tethys and Panthalassa (Grice et al., 2005; Hays et al., 2007; Kump et al., 2005; Xie et al., 2007), the extinction event has also been suggested to occur under at least locally oxic conditions in northwestern Pangea (Algeo et al., 2010; Knies et al., 2013; Proemse et al., 2013) and in the Neotethys (Korte et al., 2004; Loope et al., 2013; Richoz et al., 2010) (Fig. 1A).

Given the above, the relative timing of various environmental stresses becomes critical to understanding the role they played during the mass extinction. To address this question we examined the Festningen section in Spitsbergen (Wignall et al., 1998), a shelf sea location on northern Pangean margin during Late Permian time (Figs. 1B, 1C). The Festningen section is one of the earliest locations where development of anoxia in association with the mass extinction event was demonstrated by Wignall et al. (1998). However, that study was based on a low sample density for carbon isotope data that did not provide clarity as to detailed biogeochemical events occurring during the extinction period. Subsequent work at other sites in Spitsbergen has pointed to the gradual development of anoxia across the LPE event (Dustira et al., 2013), as well as in correlative strata in the Sverdrup Basin (Grasby and Beauchamp, 2009). To elucidate the relative timing of various environmental stressors, we have undertaken detailed analyses of the Festningen section based on high-resolution sampling through the LPE.

STUDY AREA

The Festningen section is located at Kapp Starostin, west of the mouth of Grønfjorden where it enters Isfjorden on Nordenskiöld Land, Spitsbergen (Fig. 1B). In Permian time

†E-mail: sgrasby@nrcan.gc.ca

GSA Bulletin; September/October 2015; v. 127; no. 9/10; p. 1331–1347; doi: 10.1130/B31197.1; 8 figures; 3 tables; published online 14 April 2015.

Figure 1. Location maps of field area. (A) Global Late Permian reconstruction base map, after R. Scotese (http://www.scotese.com/). (B) Location of the Festningen section on Spitsbergen. (C) Paleo-locations of important sedimentary records on the northwestern margin of Pangea at the time of the latest Permian extinction event (Embry, 1992). Bold black lines indicate present-day coastlines.

the area formed part of a broad epicontinental shelf on the northwestern margin of Pangea (Fig. 1C), along with correlative strata from the Wandel Sea (North Greenland), the Sverdrup Basin (Canadian High Arctic), and the Barents Sea and Timan-Pechora Basin (Russia) (Stemmerik and Worsley, 2005). Spitsbergen was at a paleolatitude of ~40°–45° N during the Middle to Late Permian (Golonka and Ford, 2000; Scotese, 2004).

The Festningen section occurs as ~45° eastward-dipping beds (Fig. 2) forming a ~7 km coastal section exposed in a low sea cliff, including near-continuous exposure of Carboniferous to Cenozoic strata, from Kapp Starostin to Festningsdodden. The section is located in the eastern part of the West Spitsbergen fold-and-thrust belt, an intra-continental fold-and-thrust belt ranging over more than 300 km along the west coast from the Brøgger Peninsula in the north to the Sørkapp in the very south (CASE Team, 2001; Dallmann et al., 1993; Maher and Craddock, 1988). The intense crustal shortening is a result of the northward directed movement of Greenland against the Barents shelf during the Eocene, before Spitsbergen was finally separated from Greenland. The Festningen section is part of the steeply inclined short limb of a kilometer-scale east-vergent fold structure. A sill cuts through the series (dating from the Cretaceous, 124.7 Ma) (Corfu et al., 2013). Festningen was located in the central Spitsbergen region were Upper Permian sediments, deposited in a distal shelf setting, are thickest (Wignall et al., 1998; Blomeier et al., 2013). Festningen represents the type section for both the Kapp Starostin and Vardebukta Formations which are examined here.

The Kapp Starostin Formation is a Middle to Upper Permian unit that was deposited at a time of tectonic quiescence and passive subsidence following a major relative sea-level drop coinciding with the Early Permian–Middle Permian boundary (Blomeier et al., 2013). An initial Roadian transgression led to the deposition of a widespread heterozoan carbonate (Vøringen Member), which was followed by a series of regressions and transgressions that led to the progradation of heterozoan carbonates and cherts over much of the Barents Shelf and Svalbard (Blomeier et al., 2013), as well as in the paleogeographically adjoining Sverdrup Basin (Van Hauen, Degerböls, and Trold Fiord Formations; Beauchamp et al., 2009). The uppermost fossiliferous carbonate unit in the Kapp Starostin Formation occurs ~40 m below the contact with the overlying uppermost Permian–Lower Triassic Vardebukta Formation. The topmost part of the Kapp Starostin Formation is dominated by spiculitic chert, an interval that is in part Late Permian in age (Blomeier et al., 2013) and considered equivalent to the Black Stripe and Lindström Formations of the Sverdrup Basin (Beauchamp et al., 2009).

The Vardebukta Formation is a unit of shale, siltstone, and minor sandstone that is devoid of carbonate and chert. The formation is mostly Early Triassic (Griesbachian–Dienerian) in age as shown by ammonoid and conodont fauna (Mørk et al., 1982; Nakrem et al., 2008; Tozer and Parker, 1968). While the contact between the Kapp Starostin and Vardebukta Formations was for many years considered the Permian-Triassic boundary (PTB) (e.g., Mørk et al., 1982; Mangerud and Konieczny, 1993), it is now widely accepted that the basal beds of

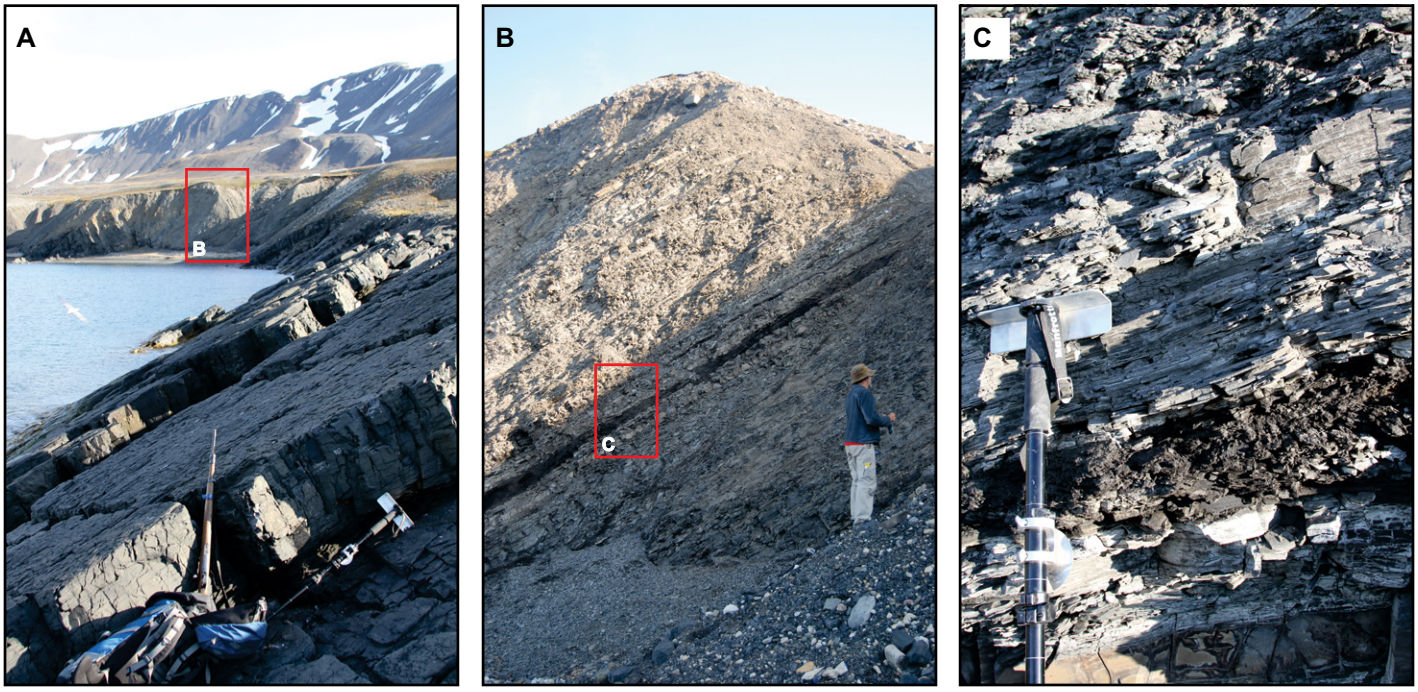

Figure 2. Field photographs of the Festningen section. (A) Top resistant bedding plane of the Kapp Starostin Formation and overlying sediments of the Vardebukta Formation. (B) Basal shales of the Vardebukta Formation (location shown in A). (C) Close-up of finely laminated shales that mark the loss of burrowers in the section (location shown in B).

the Vardebukta Formation are latest Permian (Changhsingian) in age. While *Hindeodus parvus*—the globally recognized fossil for the base of the Triassic as documented at the PTB global stratotype section and point at Meishan, China (Yin et al., 2001)—has yet to be recovered in the basal Vardebukta Formation at Festningen, chemostratigraphic considerations have led Wignall et al. (1998) to place the PTB ~6 m above the Kapp Starostin–Vardebukta contact based on the stratigraphic position of the globally recognized $\delta^{13}C$ minimum, a practice since followed by others (e.g., Dustira et al., 2013). In the Sverdrup Basin, *H. parvus* was recovered 31.75 m above the base of the Blind Fiord Formation—the stratigraphic and lithological equivalent to the Vardebukta Formation—at the Otto Fiord South section on northwestern Ellesmere Island (Henderson and Baud, 1997), while at West Blind Fiord, southwestern Ellesmere Island, the PTB is believed to occur ~12.5 m above the base of the Blind Fiord Formation (Algeo et al., 2012), based on the presence *of Clarkina taylorae* which occurs higher up in the section; *C. taylorae* is considered concurrent with *H. parvus.* At both Sverdrup localities, typical late Changhsingian conodonts have been recovered from the basal few meters of the Blind Fiord Formation (Henderson and Baud, 1997; Beauchamp et al., 2009; Algeo et al., 2012).

Wignall et al. (1998) showed a stepwise loss of fauna at Festningen as summarized here. The majority of carbonate-secreting taxa was lost ~12 m below the top of the Kapp Starostin Formation. The brachiopod fauna present in the uppermost beds may represent an early to late Lopingian age (Nakamura et al., 1987). After loss of carbonate fauna, siliceous sponges were the only taxa that remained abundant to the top of the formation. However, ichnofabrics indicating the persistent presence of soft-bodied fauna are also abundant. The top of the Kapp Starostin Formation coincides with the loss of siliceous sponges and an abrupt change in ichnofabrics, marked by disappearance of *Zoophycos* and *Chondrites*. The basal 5 m of the Vardebukta Formation is characterized by *Planolites* and pyritized small burrows, above which sediments become finely laminated and lacking in trace fossils.

Change is also observed in the terrestrial environment as indicated by palynological assemblages at Festningen (Mangerud and Konieczny, 1993). The uppermost Kapp Starostin Formation is dominated by a variety of pollen and spores from gymnosperms (conifers, pteridosperms, and rare cordaites) and pteridophytes. Basal rocks of the overlying Vardebukta Formation contain an overall lower diversity of palynomorphs than observed in the Kapp Starostin Formation with the exception that spores of lycopsids and bryophytes are present with greater diversity than observed in underlying strata. Pollen of gymnosperms are represented by *Lunatisporites* spp., a spore with pteridosperm affinity, and the first appearance of *Tympanicysta stoschiana* occurs in the basal Vardebukta Formation. Acritarchs (*Veryhachium* spp. and *Micrhystridium* spp.) then recover and become abundant in the Vardebukta Formation (Mangerud and Konieczny, 1993).

Acritarchs may have constituted the pioneering taxa of the planktonic oceanic realm following marine perturbation associated with the latest Permian event. Oceanic conditions may have been favorable for the development of widespread acritarch and prasinophyte blooms due to stratified ocean waters and elevated atmospheric carbon dioxide concentrations associated with volcanic activity and/or extreme oligotrophy in the mixed layer due to slow oceanic circulation (Martin, 1996; Payne and van de Schootbrugge, 2007).

METHODS

Sample Collection

Sampling was conducted at 50 cm spacing from 20 to 4 m below the top of the Kapp Starostin Formation, and then sample spacing across the LPE interval was reduced to 20 cm

from 4 m below to 18 m above the formation contact. The level from which samples were collected is reported in meters above (positive) and below (negative) the last chert bed that defines the top of the Kapp Starostin Formation. A total of 93 samples is included in this study.

In the field, weathered surfaces were removed and samples were collected from a narrow defined zone no greater than 2 cm thick. In the laboratory, any remaining weathered surfaces were removed, and fresh samples were powdered using an agate mortar and pestle and split into subsamples for subsequent analyses.

Geochemistry

Total organic carbon (TOC) was measured using a Rock-Eval 6 analyzer, with ±5% analytical error of reported value, based on repeats and reproducibility of standards run after every fifth sample (Lafargue et al., 1998). Total sulfur (TS) and total carbon (TC) were measured on a LECO 444 analyzer, with the average of three repeat measurements reported, with ±2% analytical error. Total inorganic carbon (TIC) was calculated from TC and TOC (TIC = TC – TOC). Elemental determinations were conducted on powdered samples digested in a 2:2:1:1 acid solution of H_2O-HF-$HClO_4$-HNO_3 and subsequently analyzed by PerkinElmer Elan 9000 mass spectrometer, with ±2% analytical error. Hg was measured at Geological Survey of Canada–Atlantic by LECO AMA254 mercury analyzer (Hall and Pelchat, 1997) (±10%).

Stable Isotope Analyses

Stable isotope measurements were conducted at the Isotope Science Laboratory, University of Calgary. For determination of $\delta^{13}C_{org}$, samples were washed with hydrochloric acid and rinsed with hot distilled water to remove any carbonate before determination of $\delta^{13}C$ of organic carbon. Organic $\delta^{13}C$ and $\delta^{15}N$ values for total nitrogen were measured using continuous flow–elemental analysis–isotope ratio mass spectrometry with a Finnigan Mat Delta+XL mass spectrometer interfaced with a Costech 4010 elemental analyzer. Standards were run every fifth sample. Combined analytical and sampling error for $\delta^{13}C_{org}$ and $\delta^{15}N_{org}$ is ±0.2‰.

Absolute Age Dating

Zircons were separated from bentonite layers using conventional heavy liquid and magnetic techniques at Curtin University, Perth (Australia). Zircon grains were handpicked under a binocular microscope. Together with standards BR266 (Stern, 2001) and OGC-1 (Stern et al., 2009) and NIST NBS610 glass, these zircons were mounted in 25-mm-diameter epoxy disc and then polished and coated with gold.

Zircons were imaged using cathodoluminescence (CL) techniques on a Zeiss 1555 VP-FESEM in the Centre for Microscopy, Characterization and Analysis at the University of Western Australia. Zircon analyses were performed on the SHRIMP II (sensitive high-resolution ion microprobe) at the John de Laeter Centre for Isotope Research, Curtin University, and followed standard operation procedures (Compston et al., 1984; Williams, 1998). The primary (O_2^-) ion beam was 0.7 nA on a 15 µm spot. The data were processed using the SQUID and Isoplot programs (Ludwig, 2003; Ludwig, 2009). Common Pb was subtracted from the measured compositions using the measured ^{204}Pb and a common Pb composition from the model of Stacey and Kramers (1975) at the appropriate stage of each analysis.

RESULTS

Absolute Age Dating

Two previously unreported bentonite layers ~2 cm thick were found in the basal Vardebukta Formation, 2.6 and 13 m above the top of the Kapp Starostin Formation (hereafter referred to as ash layers). The layers were isolated and collected in the field. Zircons were recovered only from the lower layer at 2.6 m above the formation boundary. The zircon grains are inclusion-free bipyramidal prisms, some of which are slightly rounded. These grains range in length from 60 µm to 100 µm, and are light brown with a few being light pink. The CL imaging shows uniform zircons with typical oscillatory zoning and composite zircons with cores overgrown by thin rims (Fig. 3A).

Twenty-one analyses were performed on thirteen zircons. Age data are presented in Table 1

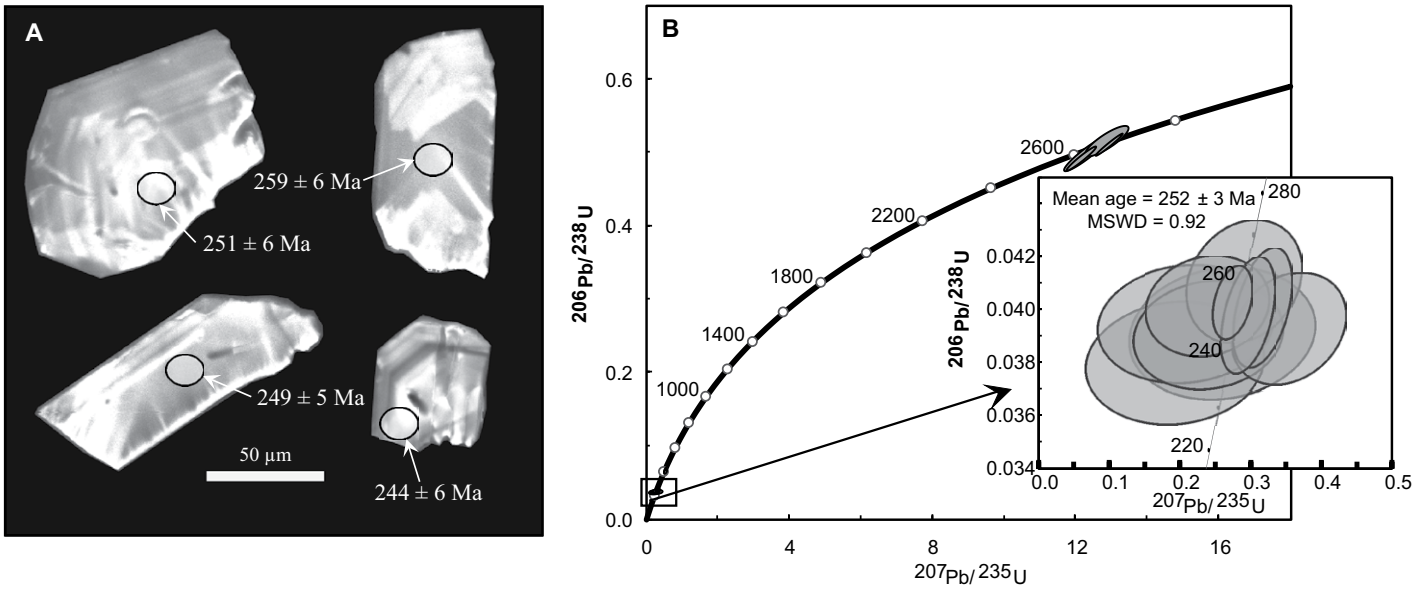

Figure 3. Results of age dating. (A) Cathodoluminescence images and ages of selected zircons of the ash layer at +2.6 m. (B) Concordia plot of sensitive high-resolution ion microprobe (SHRIMP) data for zircon grains from the ash layer (ages in Ma). MSWD—Mean square weighted deviation.

TABLE 1. SHRIMP U-Pb ZIRCON DATA FOR THE ASH LAYER

Spot	U (ppm)	Th (ppm)	f_{206} (%)	Ratios corrected for common Pb						Ages in Ma	
				$^{207}Pb^*/^{206}Pb^*$	± (%)	$^{207}Pb^*/^{235}U$	± (%)	$^{206}Pb^*/^{238}U$	± (%)	$^{206}Pb/^{238}U$	$^{207}Pb/^{206}Pb$
96A-01	137	109	0.57	0.038	24	0.21	25	0.039	2.3	253 ± 5	–
96A-02	115	60	1.77	0.065	9	0.35	9.2	0.039	2.2	244 ± 6	783 ± 189
96A-03	103	56	0.34	0.054	4.7	0.3	5.2	0.04	2.2	251 ± 6	369 ± 106
96B-01	101	56	0.75	0.057	4.9	0.32	5.4	0.04	2.3	251 ± 6	500 ± 108
96B-02r	99	49	1.25	0.048	21	0.26	21	0.039	2.6	248 ± 6	102 ± 486
96B-03	113	81	0.63	0.051	11	0.29	12	0.041	2.3	259 ± 6	253 ± 258
96B-02c	516	427	–	0.049	3.8	0.27	4	0.04	1.4	255 ± 3	162 ± 89
96B-06r	149	63	0.55	0.037	27	0.19	27	0.038	2.5	244 ± 5	–
96B-06c	221	120	0.49	0.043	15	0.24	15	0.04	1.9	256 ± 4	–
96B-07	165	112	0.33	0.044	18	0.24	18	0.039	2.1	249 ± 5	–
96B-08	171	192	0.16	0.056	3	0.51	3.6	0.066	1.9	412 ± 8	465 ± 67
96B-09c	558	92	1.15	0.179	0.4	12.13	1.4	0.491	1.3	2552 ± 37	2645 ± 6
96B-09r	256	130	–	0.181	1	12.86	1.9	0.515	1.6	2683 ± 49	2663 ± 17
96B-10c	1108	743	0.51	0.184	0.2	12.91	1.2	0.51	1.2	2646 ± 35	2685 ± 4
96B-10r	203	58	0.81	0.179	0.7	12.27	2.1	0.498	1.9	2591 ± 55	2642 ± 12
96B-08b	153	170	–	0.055	3	0.52	3.6	0.069	2	428 ± 8	425 ± 68

Note: SHRIMP—Sensitive high-resolution ion microprobe. Ages are quoted As $^{206}Pb/^{238}U$ dates for Paleozoic zircons and as $^{207}Pb/^{206}Pb$ dates for Archean zircons. Analytical results are for the lower ash layer at +2.6 m. The terms f_{206} and Pb* indicate the common and radiogenic Pb proportions, respectively.

with 1σ precision. Six of the 21 analyses were rejected due to high common lead, and 16 analyses yielded concordant or nearly concordant ages ranging from 244 Ma to 2685 Ma (Fig. 3B). Ten concordant or nearly concordant analyses plot in one single population with a weighted mean $^{206}Pb/^{238}U$ age of 252 ± 3 Ma (mean square weighted deviation = 0.92) (Fig. 3B). There are also six older ages: two Late Silurian–Early Devonian (412 ± 8 and 428 ± 8 Ma), and four Neoarchean (2645 ± 6,2663 ± 17, 2642 ± 12, and 2685 ± 4 Ma).

Carbon Isotope Records

Given the lack of carbonates, the organic carbon isotope record was examined at the Festningen section. At 15 m above the Kapp Starostin Formation contact, shales show visible signs of thermal alteration from an overlying Cretaceous sill that starts at ~19 m. Thermal effects can also be observed in the geochemical record close to the sill itself, although there is no apparent impact on the key part of the section in the basal 15 m of the Vardebukta Formation (Fig. 4). Rock-Eval 6 results in the basal 15 m provide an average T_{max} value of 453 °C, indicating that organic matter in the shales is not thermally affected by the overlying sill, and that away from the localized thermal affects, the Festningen section has never been heated past the upper end of the oil window (note T_{max} values reflect relative, not actual, burial temperatures). At the equivalent maximum burial temperatures, the stable isotope values of organic carbon are not altered (Hayes et al., 1983). The oxygen index derived from Rock-Eval analyses has an average value of 28, consistent with well-preserved organic matter.

The $\delta^{13}C$ record of the organic carbon shows two initial minor negative shifts of 1‰–2‰ at –12 m (where calcareous shelly macrofauna are lost), and then again at –3 m (Fig. 4A; Table 2). There is a brief positive shift in $\delta^{13}C$ values just below the Kapp Starostin–Vardebukta contact. The top of the Kapp Starostin Formation is marked by onset of a progressive ~8‰ negative shift in $\delta^{13}C$ over the basal 5 m of the Vardebukta Formation to a low of –33‰. This $\delta^{13}C$ low is coincident with the level where bioturbation disappears (Wignall et al., 1998). The $\delta^{13}C$ values then remain relatively stable for the next 10 m, after which there are thermal effects due to the overlying sill (Fig. 4).

Overall organic carbon content is low, with values <0.8% TOC throughout the studied interval (Fig. 4B). In the interval from –20 to –12 m, TOC values vary around 0.5%–0.6%. TOC values then drop at the level associated with loss of calcareous macrofauna (~12 m below the top of the Kapp Starostin Formation) to values around 0.4%. The TOC remains at these values for the remaining 12 m of the Kapp Starostin Formation. Above the Kapp Starostin Formation, there is a progressive drop in TOC associated with the drop in $\delta^{13}C_{org}$ values until the first ash layer at +2.6 m, where there is an abrupt increase in TOC to values of 0.5% above this level. TOC then fluctuates for the rest of the section, with peak values of 1.03% at +8.2 m.

The TIC record is plotted in Figure 4C. Even in the basal part of the section, where carbonate fossils are observed, TIC is still low (~0.5%). Above the loss of shelly macrofauna TIC values drop to <0.1% for the remainder of the Kapp Starostin Formation. Above the formation contact, there is a progressive increase in TIC to values of ~1% over the zone where $\delta^{13}C_{org}$ values drop. The TIC values then remain relatively constant to the zone of thermal influence from the overlying Cretaceous sill where they drop again. The one exception is peak values >2.5% around +8 m, coincident with a zone of peak TOC values (Fig. 4).

Redox Proxies

Several trace elements have been shown to be useful proxies for marine redox state (Mo, U, V) in addition to pyrite-associated Fe (Fe_{py}) (Scott and Lyons, 2012; Tribovillard et al., 2006). The variation of these proxy elements is plotted in Figure 5. Fe_{py} values are consistently low (<0.5%) in the upper Kapp Starostin Formation, through the zone of the last carbonate producers, and across the formation boundary as marked by the loss of sponges (Fig. 5A). Pyrite is rare until above the first ash layer at +2.6 m, after which there is a significant increase in Fe_{py} to values above 1%. This increase in pyrite is seen also in a plot of TS versus TOC (Fig. 6A). Here samples below the ash bed from both the Kapp Starostin and Vardebukta Formations plot close to the oxic-suboxic boundary as defined for ancient sediments (Raiswell and Berner, 1985). Samples above the ash layer show significantly higher Fe_{py} values, with peak levels in the finely laminated black shale at ~+8 m (Fig. 5A). In general, Fe_{py} values show a trend inverse to that of $\delta^{13}C_{org}$ (Fig. 6B) across the boundary.

The Mo concentrations in the Kapp Starostin and the basal Vardebukta Formations (solid circles in Fig. 5B) are consistently lower than average marine shale values, relative to post-Archean average Australian shale (PAAS) (Taylor and McLennan, 1985). However, Mo values increase to >20 ppm within a narrow interval of the laminated black shale at ~+8 m (Figs. 2B, 2C, 5B). A similar trend is observed in U and V data (dots in Figs. 5C, 5D). Through the upper Kapp Starostin Formation and basal Vardebukta Formation, U and V concentrations are consistently below PAAS values (except peaks associated with the first ash layer). While there is an initial minor increase at the Kapp Starostin–Vardebukta contact, values do not consistently exceed PAAS values until after the level where burrowing

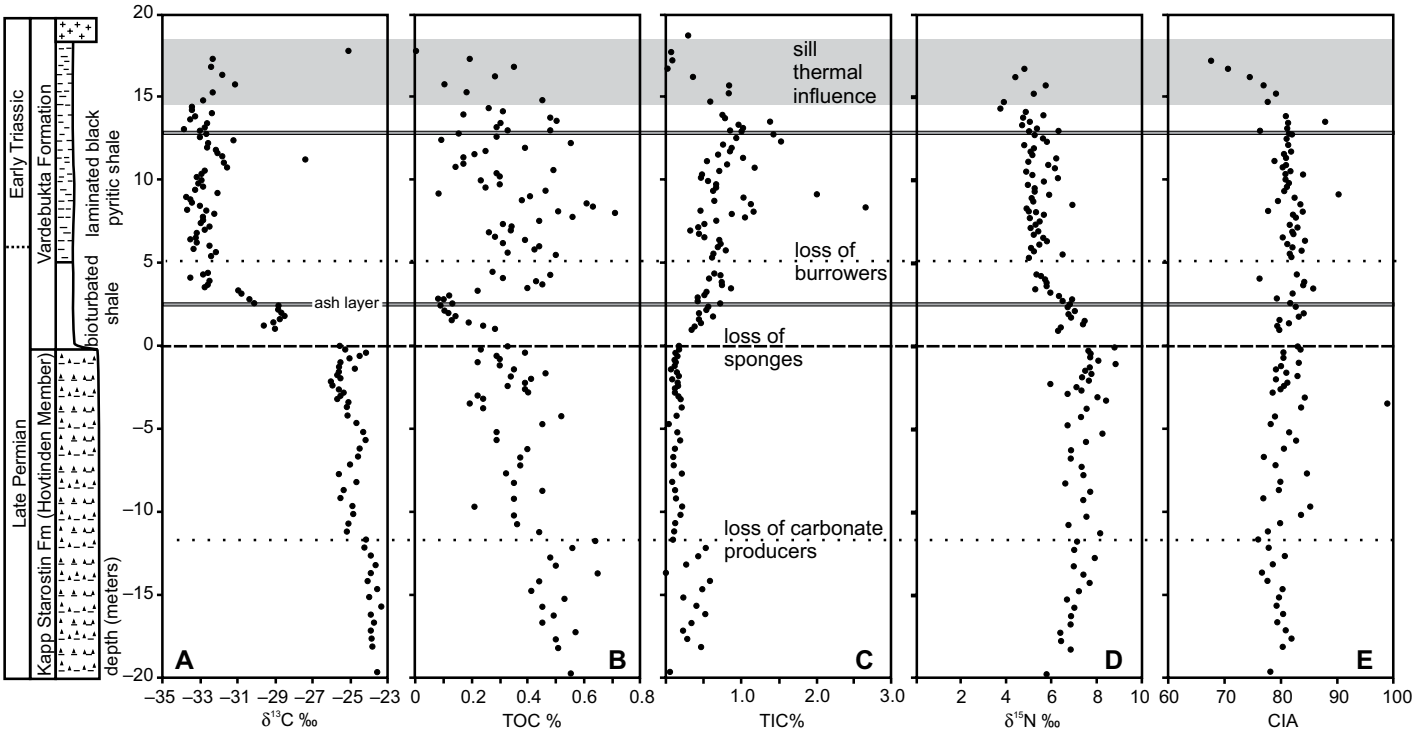

Figure 4. Plots of geochemical data from Festningen. (A) $\delta^{13}C$ of organic carbon. (B) Total organic carbon (TOC). (C)Total inorganic carbon (TIC). (D) Nitrogen isotope values. (E) Chemical index of alteration (CIA) (Nesbitt and Young, 1982). Values on left side represent sample depth in meters relative to the top of the Kapp Starostin Formation (zero point).

organisms are lost (~5 m above the formation contact). The U and V concentrations peak in the same laminated black shale ~+8 m where Mo and TOC values are also highest.

Given the change from chert to shale at the formation boundary, redox-sensitive elements were also normalized to Al to account for potential lithologic affects (gray dashed lines in Fig. 5). As with absolute values, Al-normalized values show a decline (Mo, U) in the lower Vardebukta Formation, or remain at low values (V) relative to the underlying Kapp Starostin Formation chert. The only significant increase in the metal/Al ratio is associated with the laminated black shale interval at +8 m.

Trace Metals

The variability in trace metal concentrations (Cu, Pb, As, Co, Ni, Hg) is illustrated in Figure 7. Except for Hg, absolute concentrations are plotted (dots) along with values normalized to Al (gray lines) to account for potential lithologic changes. Mercury deposition over geologic time is strongly controlled by organic matter (Grasby et al., 2013b), and therefore anomalous Hg deposition is best observed by normalizing relative to TOC (Sanei et al., 2012). Similarly, Ni is strongly scavenged by organic matter (Tribovillard et al., 2006) and is also normalized relative to TOC. Trace metal concentrations in the lowest chert-dominated portion of the section are relatively constant and below PAAS values (vertical dotted lines in Fig. 7). At –12 m, where the section is marked by the final disappearance of calcareous macrofauna, there is a small but distinct shift to lower concentrations of all metals as the lithology transitions from shaly chert to pure chert. However, there is no notable shift in normalized values at this level. The metals (concentrations and ratios) remain at low levels to the top of the Kapp Starostin Formation. In the basal 5 m of the Vardebukta Formation there is a significant increase in all trace metals to concentrations well above PAAS. This increase is also observed in the Al-normalized values. The Ni/TOC and Hg/TOC ratios also show a significant spike in the basal Vardebukta Formation. After this trace metal spike, there is a gradual decline to concentrations near or below PAAS. One exception is a brief increase associated with a zone defined by high Mo concentrations at ~+8 m, where there is also a peak in TOC values (Fig. 7). In general, trace metals in the basal Vardebukta Formation show much greater variability than in the upper portion of the Kapp Starostin Formation.

Nitrogen Isotopes

The $\delta^{15}N$ of total nitrogen has been used to assess changes in nutrient cycles across the LPE (Knies et al., 2013; Schoepfer et al., 2013). Major changes in nutrient cycling, through shifts in denitrification and/or atmospheric nitrogen fixation, can strongly influence the $\delta^{15}N$ signal of the marine nitrate pool. For the levels of thermal maturity found in the Festningen section, there are negligible effects on the stable isotope values of N (Ader et al., 1998; Bebout and Fogel, 1992). The $\delta^{15}N$ values of total N are illustrated in Fig. 4D. Results show that through the Kapp Starostin Formation the $\delta^{15}N$ values are consistently around 7‰. There is then a progressive decline in $\delta^{15}N$ values through the basal 5 m of the Vardebukta Formation to the stratigraphic level at which bioturbation was lost, above which values remain consistently around 5‰.

Chemical Index of Alteration

The chemical index of alteration (CIA) (Nesbitt and Young, 1982) provides a proxy for the degree of chemical weathering as recorded in siliciclastic sedimentary rocks, whereby increased chemical weathering mobilizes Na, K, and Ca during the transformation of feldspar

TABLE 2. GEOCHEMICAL DATA FROM THE FESTNINGEN SECTION

Sample number	Depth (m)	$\delta^{15}N$ (‰)	$\delta^{13}C$ (‰)	TOC (%)	TIC (%)	TC (%)	TS (%)	Fe_{py} (%)	Mo (ppm)	Cu (ppm)	Pb (ppm)	Ni (ppm)	Co (ppm)	As (ppm)	U (ppm)	V (ppm)	Hg (ppb)	Al (%)	CIA
GQA12-1-39	–19.7	5.8	–23.6	0.55	0.05	0.605	0.253	0.220	0.46	11.44	9.17	48.2	7.2	3	1.9	91	33	4.67	95.7
GQA12-1-40	–18.2	6.9	–23.86	0.51	0.47	0.979	0.248	0.216	0.8	11.3	7.78	43.4	6.5	3.3	2.3	77	28	4.19	77.8
GQA12-1-41	–17.7	6.4	–23.88	0.50	0.28	0.785	0.330	0.288	0.97	11.58	8.73	46.5	7	2.7	1.8	82	30	4.18	88.4
GQA12-1-42	–17.2	6.4	–23.9	0.57	0.23	0.797	0.408	0.356	1.26	10.86	9.24	53.8	6.7	4.2	2.1	78	33	3.97	89.2
GQA12-1-43	–16.7	6.9	–23.7	0.45	0.35	0.798	0.259	0.226	0.52	8.73	6.67	38.8	5.3	3.1	2	66	28	3.69	80.9
GQA12-1-44	–16.2	6.9	–24.0	0.49	0.52	1.014	0.302	0.263	0.7	10.97	7.26	50	6.4	3	2.4	75	29	4.2	75.7
GQA12-1-45	–15.7	7.0	–23.3	0.45	0.41	0.856	0.352	0.307	0.66	11.32	9.31	44.5	7	3.1	2.1	85	31	4.62	81.7
GQA12-1-46	–15.2	6.7	–24.0	0.53	0.23	0.761	0.280	0.244	0.74	10.93	8.53	50.2	5.6	3.3	2.1	79	30	4.08	87.9
GQA12-1-47	–14.7	7.2	–23.6	0.41	0.48	0.894	0.241	0.210	0.34	11.81	7.24	42.3	6.1	3.1	1.9	77	30	4.35	77.8
GQA12-1-48	–14.2	7.7	–24.1	0.44	0.59	1.025	0.258	0.225	0.33	11.53	7.89	43.7	5.9	3.4	1.7	74	32	4.07	71.3
GQA12-1-49	–13.7	7.4	–23.9	0.65	0.00	0.637	0.214	0.187	0.22	12.41	11.86	50.3	6.6	3.5	2.2	106	38	5.28	98.1
GQA12-1-50	–13.2	7.0	–23.7	0.50	0.27	0.769	0.292	0.255	0.31	11.15	9.83	46.3	6	3.4	1.9	92	34	4.7	87.2
GQA12-1-51	–12.7	7.9	–24.0	0.48	0.43	0.910	0.381	0.332	0.63	12.13	10.64	49.8	7.2	4	1.9	89	33	4.7	81.3
GQA12-1-52	–12.2	7.0	–24.3	0.56	0.53	1.090	0.366	0.319	0.57	12.21	11.82	58.9	7.7	5.9	2.3	104	37	5.4	78.2
GQA12-1-53	–11.7	7.1	–24.2	0.64	0.09	0.735	0.323	0.281	0.59	13.51	13.84	64.9	8.6	4.3	2.2	118	38	5.58	93.8
GQA12-1-54	–11.2	8.2	–25.2	0.44	0.11	0.549	0.136	0.119	0.44	7.98	4.59	40.1	4.2	2.7	2.1	85	14	3.85	91.5
GQA12-1-55	–10.7	6.8	–25.1	0.36	0.12	0.483	0.178	0.155	0.69	9.28	6.27	49.2	5.7	3.1	2.5	95	13	4.19	93.9
GQA12-1-56	–10.2	7.6	–24.9	0.35	0.19	0.543	0.216	0.188	1.13	10.21	10.12	52.7	7.2	3.6	2.5	77	13	3.6	91.0
GQA12-1-57	–9.7	n.d.	–24.9	0.21	0.22	0.427	0.187	0.163	0.73	6.31	5.07	35.2	5.2	2.3	1.5	43	13	2.5	84.3
GQA12-1-58	–9.2	7.4	–25.5	0.35	0.13	0.485	0.338	0.295	0.83	10.36	7.2	43.9	7.1	4.4	2.6	86	17	4.2	94.0
GQA12-1-59	–8.7	7.7	–25.4	0.45	0.12	0.572	0.211	0.184	1.01	11.08	10.97	55.2	8.5	3.5	2.8	87	14	3.92	93.6
GQA12-1-60	–8.2	6.6	–24.7	0.35	0.08	0.434	0.186	0.162	0.68	8.74	7.49	51	5.3	4	2.5	72	16	3.69	96.1
GQA12-1-61	–7.7	7.4	–25.6	0.32	0.21	0.531	0.217	0.189	0.73	7.57	6.9	52	6.3	3.1	2.1	57	13	3	88.2
GQA12-1-62	–7.2	7.3	–25.0	0.37	0.10	0.475	0.214	0.186	0.48	7.66	5.66	38.2	4.1	3.6	2.2	58	15	3.32	93.1
GQA12-1-63	–6.7	6.9	–24.6	0.37	0.10	0.469	0.083	0.072	0.63	11	10.05	32.8	7.4	3.7	2.2	63	16	3.2	93.5
GQA12-1-64	–6.2	6.9	–24.5	0.40	0.12	0.519	0.117	0.102	0.48	8.61	7.28	46.1	6.4	3	1.9	62	13	3.42	93.3
GQA12-1-65	–5.7	7.5	–24.3	0.29	0.19	0.479	0.108	0.094	0.29	8.67	6.61	37.5	4	1.9	1.9	64	13	3.37	92.5
GQA12-1-66	–5.2	8.3	–24.3	0.29	0.15	0.442	0.214	0.187	0.45	7.61	6.72	37	5.7	3.2	1.8	58	16	3.11	92.5
GQA12-1-67	–4.7	6.7	–24.7	0.45	0.04	0.487	0.038	0.033	0.38	7.63	6.08	46.8	4.1	2.1	2	80	9	4	97.1
GQA12-1-68	–4.2	7.3	–25.2	0.52	0.14	0.662	0.247	0.215	0.76	8.76	10.83	36.1	5.3	3	3.1	75	14	3.22	92.2
GQA12-1-69	–3.7	7.6	–25.2	0.24	0.21	0.451	0.193	0.168	0.79	9.07	6.39	33.9	4	2	1.5	51	14	2.89	89.0
GQA12-1-70	–3.2	8.4	–25.7	0.24	0.20	0.435	0.221	0.193	0.84	6.77	5.82	29.8	4.1	3	1.6	45	17	2.67	89.3
GQA12-1-71	–3	8.0	–25.5	0.22	0.17	0.388	0.251	0.219	0.72	6.49	5.87	31.4	5.4	3.4	1.4	45	16	2.77	91.9
GQA12-1-72	–3.45	n.d.	–25.1	0.19	4.98	5.167	0.034	0.030	2.92	6.09	10.07	25.2	5.3	4.9	1	27	15	1.66	12.3
GQA12-1-73	–2.8	6.7	–25.3	0.40	0.12	0.521	0.357	0.311	0.62	9.48	10.09	42.2	6.7	6.5	2.1	84	22	4.48	94.4
GQA12-1-74	–2.6	7.3	–25.7	0.39	0.13	0.518	0.342	0.298	0.82	9.15	8.68	38.9	6.5	4.9	2.2	79	19	4.04	93.3
GQA12-1-75	–2.4	7.1	–25.9	0.33	0.16	0.492	0.392	0.341	0.96	8.44	8.51	35.2	6.2	5	2.1	77	18	3.84	93.0
GQA12-1-76	–2.2	6.0	–26.1	0.39	0.16	0.546	0.474	0.413	0.92	8.91	9.81	45.9	8.2	8.1	2.6	77	24	3.83	92.8
GQA12-1-77	–2	7.7	–25.6	0.41	0.08	0.494	0.163	0.142	0.6	7.66	6.98	37	4.7	4.9	2.6	78	19	3.84	93.5
GQA12-1-78	–1.8	7.4	–25.7	0.34	0.17	0.512	0.191	0.166	0.8	7.92	9.58	32.4	5.6	4.7	2.4	66	15	3.57	92.0
GQA12-1-79	–1.6	7.8	–25.6	0.46	0.15	0.607	0.218	0.190	0.89	9.26	11.36	38.9	5.7	4.7	2.7	79	17	3.9	92.9
GQA12-1-80	–1.4	7.5	–24.8	0.35	0.05	0.399	0.079	0.068	0.36	8	7.41	33.5	4.5	4.8	2.3	80	18	4.17	95.6
GQA12-1-81	–1.2	7.7	–25.6	0.30	0.12	0.416	0.271	0.236	1.14	8.84	13.61	39.4	8.3	7	2.5	74	24	3.65	93.4
GQA12-1-82	–1	8.8	–25.5	0.22	0.13	0.347	0.211	0.184	1.31	7.21	9.52	40.3	6.8	5.2	2.1	62	15	3.5	92.2
GQA12-1-83	–0.8	8.1	–25.1	0.30	0.10	0.402	0.247	0.215	0.75	6.77	7.47	41.3	5.8	4.4	2.2	76	18	3.82	93.1
GQA12-1-84	–0.6	7.7	–24.5	0.29	0.15	0.445	0.179	0.156	0.41	6.76	7.41	30.1	4.2	4	2.2	73	20	3.43	91.0
GQA12-1-85	–0.4	7.7	–24.2	0.39	0.13	0.524	0.169	0.147	0.77	9.5	8.39	33.5	5.2	3.3	2.4	83	21	4.33	92.4
GQA12-1-86	–0.2	7.6	–25.3	0.23	0.17	0.403	0.133	0.116	0.57	7.58	5.46	27.6	3.9	3.5	2.1	65	16	3.42	91.5
GQA12-1-87	0	8.8	–25.5	0.33	0.18	0.511	0.258	0.225	1.37	7.73	7.48	36.1	5.9	4.6	2	68	20	3.33	89.6
GQA12-1-88	1	6.3	–29.0	0.28	0.34	0.623	0.522	0.455	0.48	21.09	24.68	58.7	18.8	22.7	2.3	189	29	7.98	93.2
GQA12-1-89	1.2	6.4	–29.6	0.24	0.38	0.622	0.599	0.522	1.07	38.91	34.93	83.4	23.9	29.4	3.3	143	43	8.21	87.5
GQA12-1-90	1.4	7.4	–29.1	0.19	0.47	0.656	0.608	0.530	1.34	26.77	33.78	80.8	24.2	28	2.2	138	48	8.69	92.2
GQA12-1-91	1.6	7.5	–28.8	0.13	0.43	0.564	0.380	0.331	1.21	21.12	26	88.7	19.5	24.8	3.2	125	33	8.45	85.6
GQA12-1-92	1.8	6.9	–28.6	0.14	0.63	0.774	0.384	0.334	0.28	33.42	29.48	55.4	16.2	25.4	2.2	124	27	8.25	90.1
GQA12-1-93	2	6.8	–28.7	0.11	0.44	0.551	0.335	0.292	0.52	22.69	21.79	88.8	22.6	27.3	2	135	26	8.52	92.4
GQA12-1-94	2.2	7.0	–28.8	0.10	0.54	0.638	0.218	0.190	0.14	26.74	16.63	57.6	15.8	18.4	1.9	122	16	8.57	91.3
GQA12-1-95	2.4	6.7	–28.9	0.09	0.56	0.654	0.298	0.260	0.16	16.23	16.03	54.3	17.3	20.4	2.1	126	20	8.57	91.0
GQA12-1-96	2.6	6.8	–30.1	0.13	0.72	0.852	0.449	0.392	0.46	51.12	19.95	44.5	15.7	11.3	4.9	187	30	9.98	86.9
GQA12-1-97	2.8	6.5	–30.4	0.10	0.42	0.524	0.199	0.173	0.14	53.95	6.93	74.1	27	8.3	1.4	138	17	7.85	92.1
GQA12-1-98	2.9	6.9	–30.3	0.08	0.43	0.506	0.328	0.286	0.46	123.5	9.58	76.8	43	7.5	3.3	205	25	9.5	89.1
GQA12-1-99	3.1	6.3	–30.8	0.12	0.51	0.632	0.235	0.205	0.17	38.79	12.42	58.9	18.2	8.9	1.7	121	25	7.87	91.0
GQA12-1-100	3.3	6.0	–31.0	0.22	0.54	0.760	0.489	0.426	0.16	34.6	11.71	61.9	24.5	8.7	1.8	133	27	8.2	90.7
GQA12-1-101	3.5	5.3	–32.8	0.40	0.87	1.266	1.765	1.539	0.55	68.41	32.48	100.6	64.7	12.5	1.6	159	41	7.96	85.0
GQA12-1-102	3.7	5.8	–32.6	0.45	0.75	1.196	1.819	1.586	0.96	55.11	41.35	102.9	51.2	13.1	2.4	172	43	8.09	87.7
GQA12-1-103	3.9	5.8	–32.5	0.43	0.73	1.164	1.762	1.536	0.57	62.89	32.02	88.8	34.1	9.6	2.4	145	42	8.21	88.8
GQA12-1-104	4.1	5.7	–33.5	0.31	0.57	0.884	2.422	2.112	4.4	193.7	30.95	97.6	48.4	12.1	1.8	303	77	9.75	85.1
GQA12-1-105	4.3	5.5	–32.8	0.48	0.73	1.206	1.644	1.434	1.59	57.28	30.54	68.2	23	13.6	2.4	158	60	7.87	87.6
GQA12-1-106	4.4	5.3	–32.6	0.27	0.64	0.915	1.775	1.547	0.63	44.79	21.06	61.7	21.4	11.2	2.1	134	74	8.05	90.0
GQA12-1-107	5.4	5.0	–32.5	0.50	0.62	1.124	1.590	1.386	1.43	44.41	22.67	61	21.5	12.3	2.4	144	62	7.99	88.7
GQA12-1-108	5.6	6.5	–32.2	0.33	0.63	0.963	1.405	1.225	1.23	38.04	20.04	54.6	20.4	9.5	2.3	143	53	8.19	88.2
GQA12-1-109	5.8	5.2	–33.3	0.42	0.80	1.216	1.933	1.685	2.39	64.92	23.93	68.9	29.1	12.4	3.3	161	86	9.91	87.1
GQA12-1-110	6	5.1	–32.6	0.44	0.69	1.131	1.615	1.408	0.76	48.55	23.48	63.8	22.8	10	2.9	138	69	9.66	87.8
GQA12-1-111	6.2	5.5	–33.2	0.31	0.73	1.038	1.590	1.386	0.57	45.48	23.77	61.4	24.1	9.1	2.7	136	69	9.77	86.6
GQA12-1-112	6.4	5.8	–33.6	0.39	0.71	1.104	1.589	1.385	1.04	45.25	23.53	62.1	24.9	9.7	2.7	127	60	8.47	86.3
GQA12-1-113	6.6	5.6	–33.3	0.28	0.51	0.791	1.444	1.259	0.48	40.46	18.57	56.1	23.8	6.8	2.4	136	53	10.3	89.4
GQA12-1-114	6.8	5.2	–33.2	0.26	0.44	0.699	1.423	1.240	0.35	42.11	15.11	60.1	18.8	8.2	2.5	134	46	10.97	92.2
GQA12-1-115	7	5.4	–32.8	0.34	0.32	0.664	1.666	1.452	0.44	56.96	20.9	73.1	27.3	7.3	2.6	144	53	11.28	93.8

(*continued*)

TABLE 2. GEOCHEMICAL DATA FROM THE FESTNINGEN SECTION (*continued*)

Sample number	Depth (m)	$\delta^{15}N$ (‰)	$\delta^{13}C$ (‰)	TOC (%)	TIC (%)	TC (%)	TS (%)	Fe_{py} (%)	Mo (ppm)	Cu (ppm)	Pb (ppm)	Ni (ppm)	Co (ppm)	As (ppm)	U (ppm)	V (ppm)	Hg (ppb)	Al (%)	CIA
GQA12-1-116	7.2	5.1	–32.6	0.34	0.43	0.771	1.672	1.458	0.52	47.52	21.45	72.6	25	9.5	2.9	145	51	10.92	92.1
GQA12-1-117	7.4	5.3	–33.0	0.31	0.51	0.821	1.607	1.401	0.39	49.52	18.86	66.3	26.5	6.8	4.5	137	50	10.76	90.4
GQA12-1-118	7.6	5.5	–32.9	0.44	0.67	1.110	2.129	1.856	2.76	49.23	24.83	73.6	31.5	16.3	3.5	148	81	10.02	87.3
GQA12-1-119	7.8	5.1	–32.9	0.56	1.05	1.613	1.996	1.740	5.03	44.78	25.08	71	36.4	17.5	3.4	140	77	8.99	80.6
GQA12-1-120	8	5.7	–32.3	0.71	0.88	1.587	2.001	1.745	3.91	42.37	23.33	69.6	32.1	16.1	3.7	141	82	9.56	83.7
GQA12-1-121	8.15	5.3	–32.7	0.51	1.17	1.676	1.965	1.713	5.2	39.41	20.71	61.2	26.8	13.6	3.5	131	89	7.92	78.3
GQA12-1-122	8.2	5.0	–33.7	1.03	0.46	1.490	2.830	2.467	20.65	112.2	22.51	102.8	49.4	15.5	4.5	241	134	8.74	87.4
GQA12-1-123	8.4	4.9	–33.0	0.63	2.66	3.288	2.013	1.755	10.16	39	18.33	64.1	28.8	12.8	3	117	88	7.12	63.7
GQA12-1-124	8.6	6.9	–33.5	0.61	1.13	1.740	2.644	2.306	26.37	44.64	22.58	61.5	29.8	18.9	4	129	100	7.02	76.1
GQA12-1-125	8.8	5.2	–33.6	0.38	0.65	1.025	1.918	1.672	4.51	46.76	22.26	68	32.2	12.6	3.1	147	57	9.62	86.5
GQA12-1-126	9	5.1	–33.8	0.41	1.03	1.442	1.929	1.682	3.67	55.51	19.05	72.7	37.5	11.7	2.3	156	57	9.2	80.4
GQA12-1-127	9.2	5.9	–32.1	0.08	2.01	2.090	1.230	1.073	1.58	24.06	15.44	42.6	16.8	7.1	2.6	97	25	6.99	64.7
GQA12-1-128	9.4	5.3	–33.3	0.46	0.63	1.089	2.410	2.101	2.77	47.04	25.08	75.9	40.1	13.5	3.6	150	50	9.55	88.0
GQA12-1-129	9.6	5.3	–32.8	0.25	0.67	0.919	1.345	1.173	0.59	37.53	14.5	55.1	21.4	6.1	2.6	128	38	10.06	86.7
GQA12-1-130	9.8	5.0	–33.1	0.30	0.67	0.969	1.316	1.147	0.96	33.22	17.76	56.5	19.6	7.5	2.7	133	26	9.54	86.9
GQA12-1-131	10	5.7	–32.9	0.23	0.56	0.791	2.308	2.013	0.62	74.03	20.83	77.9	28.9	6.5	2.7	165	47	10.87	89.7
GQA12-1-132	10.2	6.3	–33.2	0.30	0.47	0.766	1.833	1.598	1.02	43.74	21.65	69.7	26.2	8.4	2.8	152	35	10.63	90.9
GQA12-1-133	10.4	5.2	–33.0	0.29	0.48	0.770	1.755	1.530	1.92	37.5	23.1	70	27.6	10.1	3.1	143	30	10.99	91.3
GQA12-1-134	10.6	4.9	–32.8	0.49	0.71	1.200	2.019	1.760	1.98	43.38	23.1	63.9	23.9	8.6	3.2	123	40	9.53	87.0
GQA12-1-135	10.8	6.2	–31.6	0.14	1.18	1.320	1.314	1.146	1.42	23.69	14.81	40.3	15.2	7.1	2.3	89	19	6.76	71.7
GQA12-1-136	11	5.9	–31.8	0.17	0.81	0.985	1.532	1.335	1.4	28.36	17.77	53.2	19.9	8.7	2.8	118	23	9.02	83.1
GQA12-1-137	11.2	5.0	–27.4	1.02	0.55	1.566	2.265	1.975	1.41	56.42	22.87	73.8	36.5	9.8	2.8	130	74	9.1	87.3
GQA12-1-138	11.4	6.2	–31.8	0.17	1.03	1.197	1.653	1.441	2.14	28.58	18.85	50.1	20.9	10.6	2.7	112	34	8.21	78.5
GQA12-1-139	11.6	5.2	–32.1	0.21	0.69	0.905	1.461	1.274	0.83	24.52	19.69	48.5	18	7.4	2.9	111	23	9.45	86.3
GQA12-1-140	11.8	5.1	–32.2	0.25	0.85	1.103	1.337	1.166	1.51	30.19	18.57	56.1	19.6	11.4	3	121	31	9.31	84.1
GQA12-1-141	12	5.2	–32.6	0.39	0.87	1.256	1.808	1.576	3.08	37.18	20.51	69.1	30.4	13.4	3	130	48	9.09	83.8
GQA12-1-142	12.2	4.8	–32.6	0.55	0.76	1.311	1.909	1.664	2.9	37.2	21.61	70.1	29.5	13.4	3.1	129	56	9.23	85.3
GQA12-1-143	12.4	5.8	–31.3	0.09	1.53	1.625	1.509	1.316	1.28	30.13	12.59	43.4	17.1	5.4	2.2	96	19	6.7	66.5
GQA12-1-144	12.6	5.6	–33.1	0.29	0.94	1.226	1.667	1.454	2.55	38.62	20.28	62.6	25.2	10.5	2.7	130	34	9.55	81.8
GQA12-1-145	12.8	5.3	–32.7	0.15	1.42	1.574	1.382	1.205	3.04	23.73	14.9	44.8	17	9.6	2	85	35	6.67	69.1
GQA12-1-146	13	5.0	–33.1	0.33	1.01	1.336	1.777	1.549	7.18	31.89	20.85	56.6	24.2	14.2	2.1	110	45	7.38	78.3
GQA12-1-147	13.2	5.4	–32.8	0.29	1.03	1.316	1.758	1.533	4	31.01	19.5	57.3	22.7	19	2.2	107	47	7.1	77.5
GQA12-1-148	13.05	6.3	–33.9	0.48	0.86	1.335	2.273	1.982	12.34	199.9	8.87	57.1	40	6.9	2.3	453	41	9.75	78.6
GQA12-1-149	13.4	4.7	–32.7	0.30	0.97	1.267	1.611	1.405	4.13	26.05	18.52	54.5	22.8	14	2.5	114	34	7.19	79.2
GQA12-1-150	13.6	5.1	–33.6	0.50	1.39	1.886	1.722	1.502	4.96	28.22	19.66	57.6	22	12.6	2.6	106	42	7.1	75.1
GQA12-1-151	13.8	4.8	–33.3	0.48	0.79	1.266	1.712	1.493	3.89	30.48	20.33	62	28	13.2	2.2	117	43	7.31	83.0
GQA12-1-152	14	5.7	–32.4	0.17	0.75	0.922	1.723	1.502	2.55	28.22	20.31	55	22	12	2.2	106	35	7.44	84.3
GQA12-1-153	14.2	4.9	–33.4	0.31	5.98	6.291	0.461	0.402	3.45	16.87	12.8	34.9	14.3	7.5	1.9	56	27	4.54	37.1
GQA12-1-154	14.4	3.8	–33.5	0.26	6.11	6.369	0.948	0.827	3.5	16.01	12.1	33.4	14.5	7.4	1.9	53	24	4.57	36.7
GQA12-1-155	14.8	3.9	–32.8	0.45	0.59	1.040	1.700	1.482	2.31	36.18	23.36	66.9	34.7	11.4	2.1	115	33	7.7	83.9
GQA12-1-156	15.3	5.2	–32.4	0.18	0.84	1.017	1.300	1.133	1.71	22.35	17.36	47.7	17.2	10.2	1.8	94	15	7.25	77.8
GQA12-1-157	15.8	5.8	–31.2	0.10	0.85	0.946	0.826	0.720	0.37	24.18	17.5	55.3	17.6	7.7	2	108	10	7.99	79.0
GQA12-1-158	16.3	4.4	–31.8	0.28	0.36	0.640	1.340	1.168	1.53	30.45	32.77	62.1	22.2	11.3	1.9	115	7	7.82	89.3
GQA12-1-159	16.8	4.8	–32.4	0.35	0.02	0.371	0.053	0.046	1.27	41.1	2.32	57.4	23.1	5.9	1.8	128	1	7.98	95.1
GQA12-1-160	17.3	n.d.	–32.4	0.19	0.09	0.276	0.727	0.634	3.08	30.46	8.84	65.3	21.8	3.6	1.8	128	1	8.2	95.8
GQA12-1-161	17.8	n.d.	–25.1	0.00	0.07	0.069	0.771	0.672	3.34	34.21	11.97	51.7	20.7	2.7	1.8	129	0.43	7.79	96.3
GQA12-1-162	18.8	n.d.	n.d.	0.01	0.30	0.306	0.430	0.375	3.01	27.94	20.86	49.8	17.9	2.8	1.6	119	0.49	7.72	89.8

Note: TOC—total organic carbon; TIC—total inorganic carbon; TC—total carbon; TS—total sulfur; Fe_{py}—pyrite-associated iron; CIA—chemical index of alteration; n.d.—not determined. Sample depths are provided in meters relative to the top of the Kapp Starostin Formation (zero) as marked by the last chert bed. Negative values are below this marker and positive values above.

minerals to clays. However, the CIA needs to be corrected for potential Ca from carbonate (Fedo et al., 1995). For Festningen, the CIA shows almost no variation through the section analyzed, with values consistently near 80 (Fig. 4E). Toward the top of the section the CIA values drop within the zone of thermal influence from the overlying Cretaceous sill.

DISCUSSION

Age Dating

The bentonite layer +2.6 m had one dominant zircon age population with a weighted mean age of 252 ± 3 Ma, which we interpreted as the crystallization age of the volcanic ash. Six older ages were obtained in zircons which are slightly rounded and likely represent xenocryts (Fig. 3B). The source of these older ages may be: (1) Silurian to Early Devonian granites, located in the Nordaustlandet terrane of northeast Svalbard, whose ages range from 410 to 440 Ma (Johansson et al., 2002); and (2) a Neoarchean quartz monzonite located in the Ny-Friesland, northern Svalbard, which yielded an upper intercept of 2709 ± 28 Ma, considered the best estimate of the crystallization age (Hellman et al., 2001).

Carbon Isotope Records and the LPE Boundary

While not having sufficient precision to be definitive, the 252 Ma age of the ash layer suggests that the top of the Kapp Starostin Formation represents the global LPE boundary. This is further constrained by carbon isotope data. The organic carbon isotope record at Festningen shows a distinct negative $\delta^{13}C$ excursion initiated at the basal-most Vardebukta Formation (Fig. 4), consistent with negative excursions associated with the LPE horizon observed in inorganic carbon isotope records (Korte and Kozur, 2010). This negative carbon isotope shift is also consistent with organic carbon isotope records from other boreal settings (e.g., Sverdrup Basin [Grasby and Beauchamp, 2008, 2009]; northeastern British Columbia [Wang et al., 1994; Wignall and Newton, 2003]; East Greenland [Twitchett et al., 2001]; and Norway-Spitsbergen [Dustira et al., 2013; Hermann et al., 2010]). In their review, Korte and Kozur (2010) showed that the initial negative decline in $\delta^{13}C$ values started

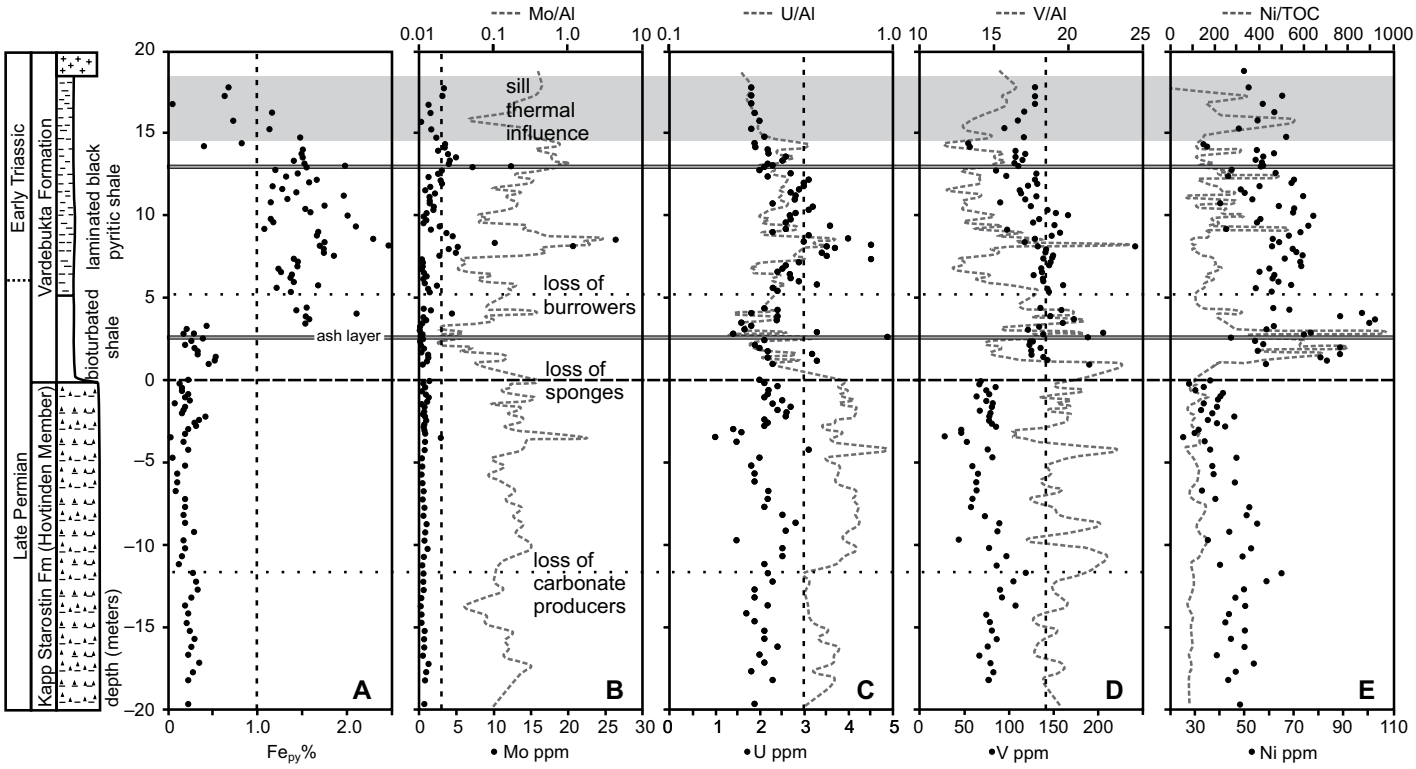

Figure 5. Plots of redox-sensitive indicators for Festningen. (A) Pyrite-associated iron (Fe_{py}). (B) Molybdenum. (C) Uranium. (D) Vanadium. (E) Nickel. Dots show absolute concentrations; gray dashed lines represent normalized values, normalized either to aluminum or to total organic carbon (TOC). Vertical black dashed lines represent average shale PAAS values.

at the LPE and reached a minimum $\delta^{13}C$ value after the extinction event. Shen et al. (2011) also showed that the negative excursion in the carbon isotope record occurs after the main extinction event in the Tethys. As well, at Meishan, Burgess et al. (2014) showed that after the initial negative peak, the broad decline in $\delta^{13}C$ values occurs after the main extinction event. Therefore, we interpret the negative shift at Festningen as being consistent with the global pattern for the negative carbon isotope excursion initiating at the LPE event. Based on this interpretation, we follow previous workers who used the $\delta^{13}C$ minimum as the approximate PTB in Spitsbergen (Dustira et al., 2013; Wignall et al., 1998), and the onset of the major $\delta^{13}C$ decline above the last chert beds to mark the LPE horizon. This makes the LPE horizon coincident with the top of the Kapp Starostin Formation, which also marks the loss of sponges as well as collapse of well-developed ichnofauna, including *Zoophycos* and *Nereites* (Wignall et al., 1998).

The top of the Kapp Starostin Formation also marks a shift in palynological assemblages, from those dominated by gymnosperms to an assemblage dominated by lycopsids, as described at Festningen and other sections on Spitsbergen (Mangerud and Konieczny, 1993). This lycopsid "spore peak" in latest Permian strata is well documented elsewhere in the Northern Hemisphere (Hochuli et al., 2010; Twitchett et al., 2001). These changes in palynoassemblages across the boundary represent major vegetation community collapse of Late Permian gymnosperm-dominated ecosystems followed by recolonization by pioneering lycopsids and bryophytes and components of typical Early Triassic shrubland communities (Hochuli et al., 2010; Twitchett et al., 2001), representing a terrestrial response to environmental stress followed by rapid, but short-lived, recovery. Twitchett et al. (2001) noted that the synchronous collapse of the marine and terrestrial ecosystems preceded a sharp negative carbon isotope excursion at the LPE boundary in East Greenland. As well, Hermann et al. (2010) showed that in the Trøndelag and Finnmark Platform, Norway, the marine extinction level was immediately followed by the increase in spore abundance and a sudden drop of C isotope values. Thus, the latest Permian terrestrial collapse observed across northwestern Pangea is coincident with the marine extinction marked by the loss of chert-forming siliceous sponges.

The loss of chert was a global feature at the LPE (Beauchamp and Baud, 2002; Beauchamp and Grasby, 2012) that has been correlated with the extinction event in Meishan (Wignall and Newton, 2003) and onset of the Early Triassic chert gap. While driven by sponge extinction, it may also represent a significant drop in silica solubility due to significant increase in ocean temperatures (Beauchamp and Grasby, 2012; Joachimski et al., 2012). Previous workers also placed the LPE boundary at the top of the last chert beds in correlative strata from the Sverdrup Basin (Embry and Beauchamp, 2008; Grasby and Beauchamp, 2008; Proemse et al., 2013) and western Canada (Schoepfer et al., 2013). However, this placement of the LPE boundary contrasts with the claims of Algeo et al. (2012) who speculated that the loss of sponges and complex ichnofabric represents an earlier extinction than the LPE event itself (their "Arctic event"). The level that they assign as the LPE horizon at the West Blind Fiord section of the Sverdrup Basin is marked by minor geochemical changes in the overlying shales (Fig. 8). These are more consistent with those observed in Festningen at the level of the first ash bed. The samples that Algeo et al. (2012) analyzed from this level at West Blind Fiord (collected by two of us, S. Grasby and B. Beauchamp) were in fact ash layers, and thus the chemistry is not representative of marine conditions as they assumed.

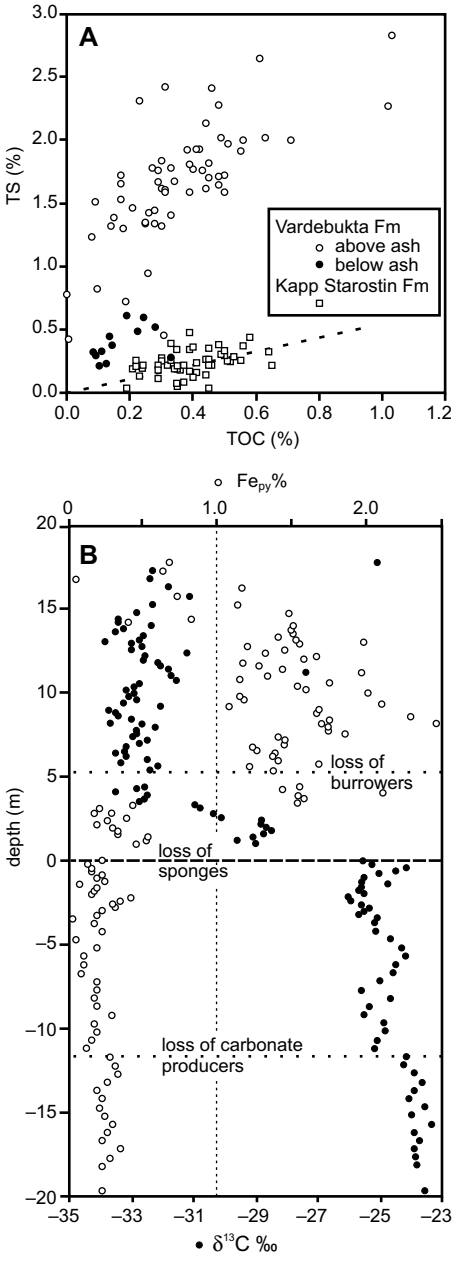

Figure 6. Geochemical plots. (A) Total sulfur (TS) versus total organic carbon (TOC) showing the significant shift to a more anoxic state above the lowest ash bed (white circles). (B) Inverse relationship between carbon isotope values and redox proxies (pyrite-associated iron [Fe_{py}] shown here) across the extinction horizon (loss of sponges). Vertical dashed line represents the Fe_{py} value reflective of transition to anoxic conditions (> 1%).

Redox Proxies

Multiple proxies for anoxia examined as part of this work, including redox-sensitive trace elements, Fe_{py}, and TOC and TS plots, show similar trends. In the chert-dominated upper Kapp Starostin Formation, redox-sensitive elements are consistently lower than average PAAS values, and TOC and TS values plot along the oxic boundary for oxic-suboxic waters. Above the Kapp Starostin Formation there is a slight shift to higher concentrations of redox-sensitive elements, however they remain below PAAS values, suggesting a largely oxic system in the basal 2.6 m of the Vardebukta Formation. Such an oxic environment is consistent with Fe_{py} that remains low through the Kapp Starostin and basal Vardebukta Formations. These data suggest then that the LPE boundary, marked by the loss of siliceous sponges, occurs under oxic to dysoxic conditions at Festningen.

Above the first ash layer at +2.6 m, TS values increase and Fe_{py} values plot in the suboxic zone of Raiswell and Berner (1985). The peak values of redox-sensitive elements, exceeding PAAS, as well as peaks in Al-normalized values occur at ~+8 m in association with the black laminated shale above the zone where burrowers are lost. These increased concentrations of redox-sensitive elements, both absolute and normalized to Al, are strong indicators of marine anoxia (Tribovillard et al., 2006), suggesting that conditions at Festningen transitioned to a more anoxic environment after the LPE boundary. This is supported by the progressive shift to lower $\delta^{15}N$ values that suggests increased fixation of atmospheric N_2, possibly in response to increasing anoxia (Schoepfer et al., 2013; Proemse et al., 2013; Knies et al., 2013). This interpretation of anoxia is consistent with original work by Wignall et al. (1998) who suggested onset of anoxia at this level, in addition to recent work by Bond and Wignall (2010) who showed pyrite framboid data at Festningen consistent with transition to anoxic conditions at the same level.

Trace Metals

A key aspect of the Festningen section is the significant increase in metals at the LPE boundary that occurs at a level where anoxia has not yet developed. In fact, metal concentrations right above the LPE are greater than when anoxic conditions eventually develop higher in the section. These high metal concentrations argue against these anomalous metal loads being associated with increased drawdown into sediment. Previously it has been suggested that metal enrichments at the LPE boundary could be related to high loading rates from the Siberian Trap eruptions (Grasby et al., 2011; Sanei et al., 2012). Similarly, we interpret the anomalous metal concentrations at the LPE boundary, both absolute and Al-normalized, to be related to enhanced metal flux from the Siberian Traps. While described here for Festningen, similar trace metal spikes have been observed in the Sverdrup Basin (Grasby et al., 2011) as well as at Meishan, where Ni concentrations show a significant increase just prior to the carbon isotope shift (Kaiho et al., 2001; Rothman et al., 2014), implying that increased metal loading at the LPE is a global phenomenon.

PROGRESSIVE ENVIRONMENTAL DETERIORATION

Results from our Festningen study demonstrate evidence for progressive environmental deterioration leading up to and across the LPE event. This can be characterized by three main events: (1) lysocline shoaling driving loss of carbonate producers, (2) volcanic metal loading related to volcanics, and (3) onset of anoxia.

Loss of Carbonate Producers

The first notable event in the Festningen section is the loss of carbonate producers (i.e., brachiopods, bivalves, corals, bryozoans, foraminifers) around 12 m below the top of the Kapp Starostin Formation (Wignall et al., 1998), marking the last appearance of any carbonate-secreting organisms prior to the LPE event. Not only are carbonate fossils absent above this point, but TIC values drop to near zero (Fig. 4), indicating a complete absence of carbonate sediment. The loss of carbonate producers is also marked by a small negative shift in $\delta^{13}C$ and drop in TOC (Fig. 4).

Early work had interpreted the loss of carbonate producers as being driven by a shift to cooler water temperatures (Beauchamp and Baud, 2002; Reid et al., 2007; Stemmerik and Worsley, 1995). However, reduced ocean temperatures are insufficient to account for loss of carbonate production in clastic-starved, well-lit, aerobic environments (Beauchamp and Grasby, 2012). As well, temperatures in the Boreal Realm were already increasing during latest Permian time (Beauchamp and Grasby, 2012) when silica producers became the dominant sediment producer. Instead, the transition from carbonate to silica factories most likely relates to lysocline shoaling driven by increasing atmospheric CO_2 (Beauchamp and Grasby, 2012). Carbon cycle modeling suggests progressive increase in atmospheric CO_2 through the Late Permian (Berner, 2006) with values as high as 4000 ppm prior to the LPE (Cui and Kump, 2014). Given the inverse solubility of $CaCO_3$ with tempera-

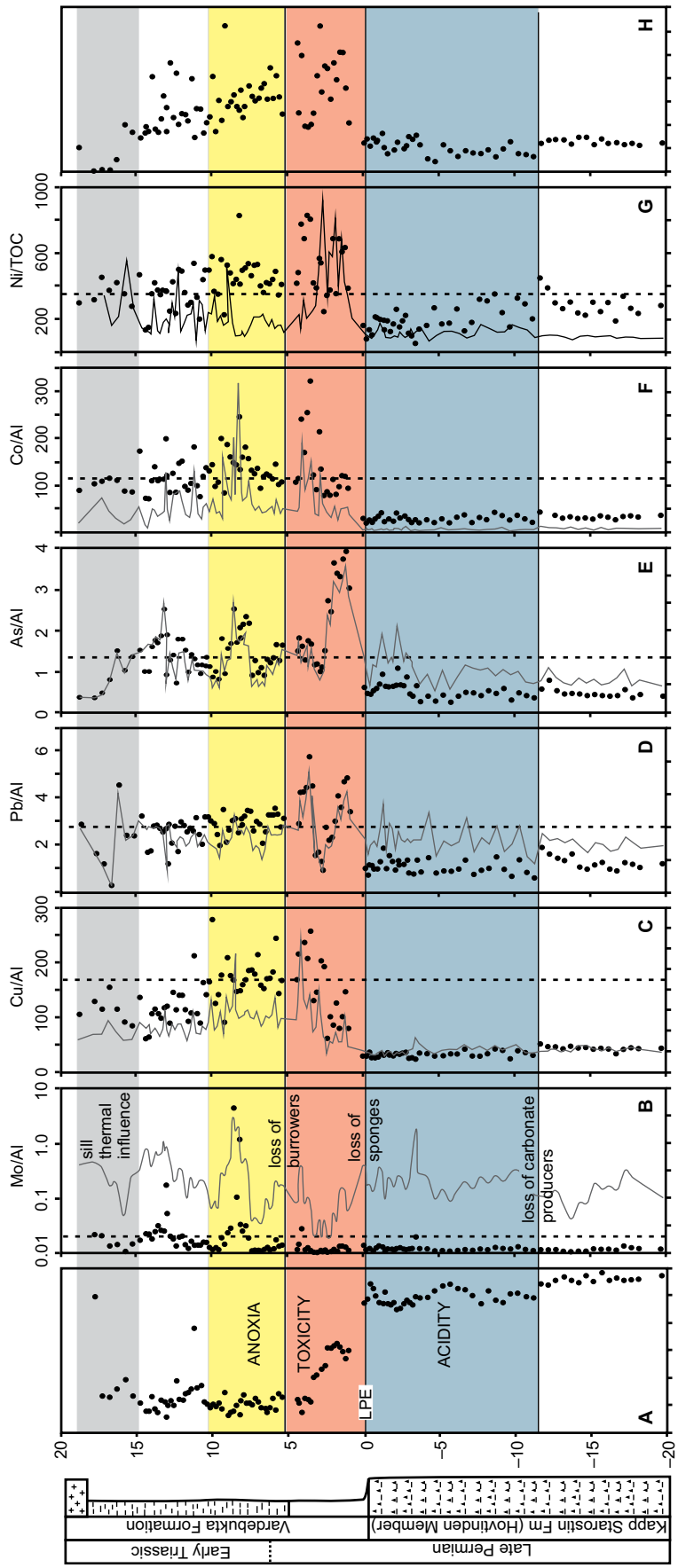

Figure 7. Plot of trace metals along with (A) carbon isotope values and (B) Mo for reference. Trends in metals across the extinction horizon shown are: (C) Cu; (D) Pb; (E) As; (F) Co; (G) Ni; and (H) Hg normalized to total organic carbon (TOC). Average shale values are shown as vertical dashed lines derived from Taylor and McLennan (1985) for Pb, Co, and Ni, and from Wedepohl (1991) for Cu and As. Colored bars represent interpreted major impacts on life across the extinction event, including initial marine water acidity, development of toxicity, then finally anoxia. LPE—latest Permian extinction. Gray lines represent the metal/Al normalized values.

ture, higher latitudes would be most susceptible to increasing atmospheric CO_2 levels, becoming undersaturated with respect to carbonates, while lower latitudes maintained shallow-water carbonate factories.

Metal Loading

The eruption of the Siberian Traps, which roughly coincides with the LPE (Burgess et al., 2014), could have had both positive and negative impact on global ecosystems through release of both nutrients and toxic metals (Frogner Kockum et al., 2006; Hoffmann et al., 2012; Jones and Gislason, 2008). Metal loading from volcanic eruptions can serve as a significant input of limiting nutrients (e.g., Fe, Ni; Boyd et al., 2000; Konhauser et al., 2009; Langmann et al., 2010), increasing primary productivity, which may relate to microbial blooms that occur at the LPE (Lehrmann, 1999; Xie et al., 2005, 2010). At the same time, high rates of metal loading could exert a toxic shock to both the marine and terrestrial systems. While increased acid rain related to the Siberian Trap eruptions has been argued to have had significant impact on the terrestrial environment (Black et al., 2014; Sephton et al., 2015), metal loading would also have been deleterious as it dramatically decreases photosynthetic efficiency in vascular plants (Odasz-Albrigtsen et al., 2000). Although there is pollen evidence for significant impact to the terrestrial system, the CIA does not change across the boundary, indicating no significant changes in chemical weathering rates as suggested for lower latitudes (Sephton et al., 2005; Sheldon, 2006). This is consistent with the work of Hochuli et al. (2010) who showed a rapid recovery of plant ecosystems from records in the southern Barents Sea, and suggested that in the Boreal Realm terrestrial impact was relatively short term.

Volcanic eruptions are associated with release of metals to the atmosphere (Vie le Sage, 1983) that can form significant components of global element cycles; e.g., volcanoes account for 40% of the modern natural component of the global Hg budget (Pyle and Mather, 2003). Volatile metals released from the magma (e.g., Cu, Zn, Ni, Pb, Cd, Hg, As) can form stable compounds (e.g., $CdCl_g$, CdS_g; Symonds et al., 1987) that condense onto ash particles, creating notable metal enrichments in ash relative to the source magma (Bagnato et al., 2013). Leaching experiments of ash fall show significant subsequent release of these metals into water (Olsson et al., 2013; Ruggieri et al., 2011). Whether the resultant dissolved concentrations can be significant enough to create toxicity, or in some cases nutrient influx (e.g., Fe), would be a

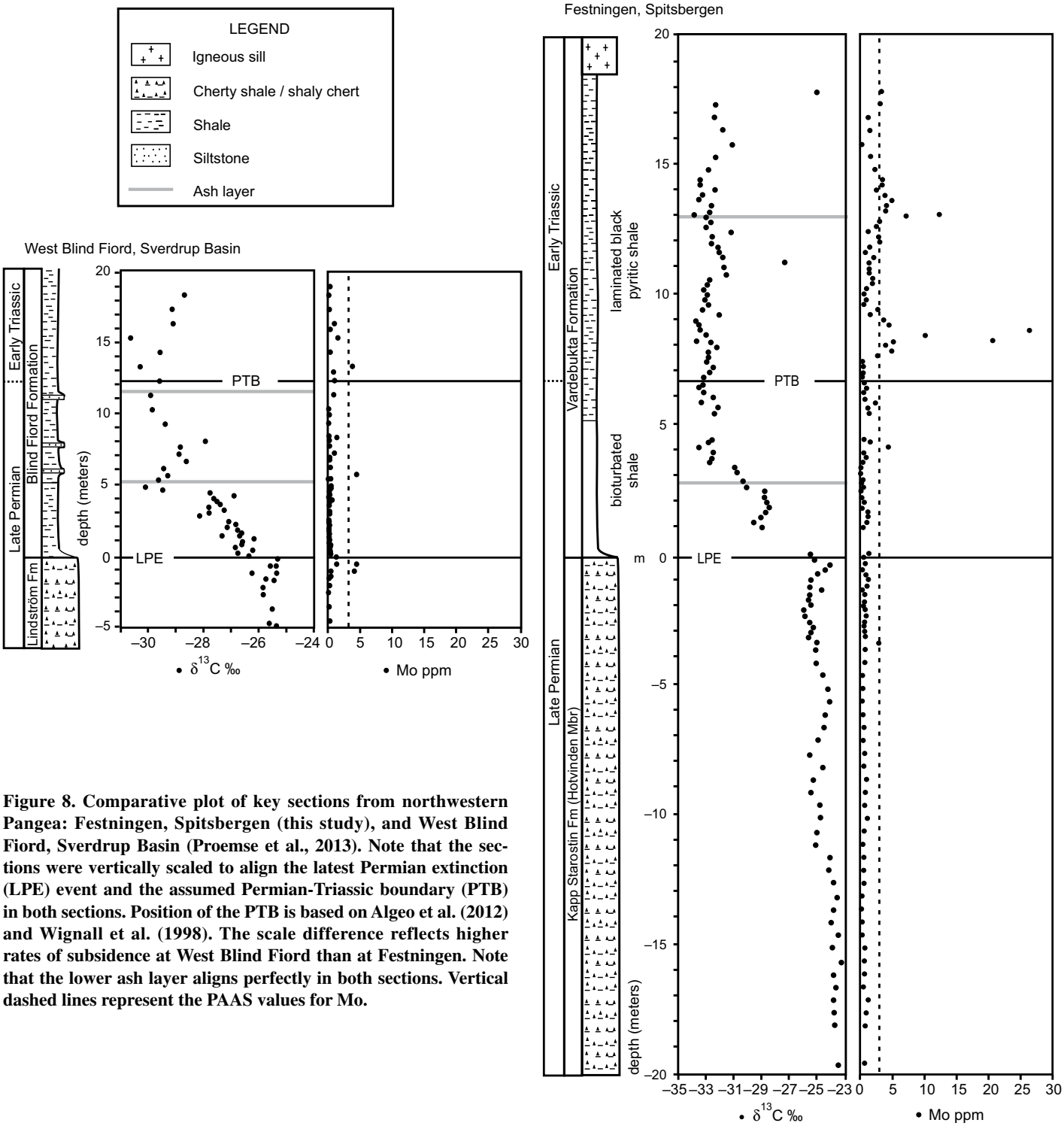

Figure 8. Comparative plot of key sections from northwestern Pangea: Festningen, Spitsbergen (this study), and West Blind Fiord, Sverdrup Basin (Proemse et al., 2013). Note that the sections were vertically scaled to align the latest Permian extinction (LPE) event and the assumed Permian-Triassic boundary (PTB) in both sections. Position of the PTB is based on Algeo et al. (2012) and Wignall et al. (1998). The scale difference reflects higher rates of subsidence at West Blind Fiord than at Festningen. Note that the lower ash layer aligns perfectly in both sections. Vertical dashed lines represent the PAAS values for Mo.

function of the ash loading rate (Olsson et al., 2013). In any case, ash loading would represent an anomalous metal load to a system that can be used as a proxy for enhanced volcanic activity in the geologic record (Grasby et al., 2011, 2013b; Sanei et al., 2012; Sial et al., 2013; Silva et al., 2013).

The Siberian Traps also intruded through the Tunguska sedimentary basin, and it has been suggested that this induced combustion of coal and organic-rich shales, causing release of over three trillion tons of carbon (Grasby et al., 2011; Korte et al., 2010; Ogden and Sleep, 2012; Reichow et al., 2009; Retallack and Jahren, 2008; Saunders and Reichow, 2009; Svensen et al., 2009). As with volcanoes, volatile metals released during combustion (e.g., Be, Zn, As, Cd, Tl, Pb, and U) condense and concentrate onto the resulting fly ash that is composed dominantly of SiO_2, Al_2O_3, and Fe_2O_3 particles (Gieré et al., 2003). The enrichment factor of metals,

relative to the source organics, can range from 30× up to 100× (Gieré et al., 2003; Klein et al., 1975; Papastefanou, 2010). Similar concentration of metals onto fly ash has been observed during combustion of oil shales (Blinova et al., 2012). Metal enrichment is much greater in the smaller size fraction, as such particles have the largest surface area for condensation of volatiles per unit mass (Davison et al., 1974; Furuya et al., 1987; Kaakinen et al., 1975b; Martinez-Tarazona and Spears, 1996; Smith et al., 1979). The smallest size fraction also has the longest atmospheric residence times, and consequently the greatest spatial distribution during atmospheric transport (Kaakinen et al., 1975a; Smith et al., 1979). Similar to volcanic ash, metals condensed onto the surface of fly ash particles are also released when ash is submerged in water (Bednar et al., 2010). Evidence for coal ash loading and metal release at the LPE was observed in the Sverdrup Basin by Grasby et al. (2011), suggesting that coal ash dispersal was widespread in the Northern Hemisphere during the latest Permian.

The largest volcanic eruption in Earth history, the Siberian Traps, combined with combustion of organics in the Tunguska Basin would have had an extremely high metal loading rate that far exceeds normal background. As an example, Sanei et al. (2012) calculated a Hg loading rate from the Siberian Traps that would be 4× modern anthropogenic emissions, assuming a 500 k.y. eruption period. Similar estimates for other metal fluxes can be made based on the metal/S ratio for modern volcanic emissions (Nriagu, 1989) and estimates of total SO_2 release of 3.8×10^{13} Mg from the Siberia Trap eruptions (Beerling et al., 2007). Averaging over an assumed maximum 500 k.y. eruption history gives a conservative minimum increase. Based on this, Siberian Trap eruptions may have increased global metal flux to the atmosphere by 9% (Se) to 78% (Co) above modern natural background flux (Mather et al., 2013; Nriagu, 1989) (Table 3). However, Siberian Trap magmatism was more likely episodic over the total eruption interval (Pavlov et al., 2011). Such episodic eruption would mean that rather than an overall average background increase, the extinction interval would be better characterized by pulses of extreme metal loading significantly higher than those estimated here. Pavlov et al. (2011) estimated that the total eruption intervals may represent as low as 8% of the total eruption history (suggesting a net ~40 k.y. for metal release). Based on this, metal flux by the Siberian Traps may have ranged from 107% (Se) to 977% (Co) above background (Table 3).

While estimates of metal loading rates related to the Siberian Traps contain uncertainties, it is interesting to note that even conservative estimates are of the same order of magnitude as modern anthropogenic metal release (Pacyna and Pacyna, 2001) that is the subject of global concern. However, higher rates based on a more likely pulsed eruption history are one to two orders of magnitude greater than modern anthropogenic emissions. Such extreme loading rates may readily explain the metal anomalies at the LPE boundary, and likely represented a toxic shock to both marine and terrestrial ecosystems.

TABLE 3. CALCULATED INCREASE IN METAL LOADING RATES DUE TO THE SIBERIAN TRAP ERUPTIONS

Element	Metal/S ($\times 10^{-4}$)	Rate, 500 k.y. (Gg/a)	Rate, 40 k.y. (Gg/a)	Natural rate (Gg/a)	500 k.y. rate increase (%)	40 k.y. rate increase (%)	Anthropogenic rate (Gg/a)
As	0.8	3.04	38	12	25	316	5
Cd	0.195	0.741	9.26	1.3	57	712	3
Co	1.255	4.77	59.6	6.1	78	977	
Cr	3.15	11	137	44	27	312	14.7
Cu	2.05	7.79	97.4	28	28	348	25.9
Hg	0.21	0.798	9.98	2.5	32	399	2.2
Mn	9.4	35.7	446	317	11	141	11
Mo	0.09	0.342	4.28	3	11	143	2.6
Ni	3.11	11.8	148	30	39	492	95.3
Pb	0.78	2.96	37	12	25	308	119.3
Sb	0.135	0.513	6.41	2.4	21	267	1.6
Se	0.21	0.798	9.98	9.3	9	107	4.6
V	1.12	4.26	53.3	28	15	190	240
Zn	2.005	7.62	95.3	45	17	211	57

Note: Two loading rates are calculated: for a constant eruption rate over 500 k.y., and a sporadic eruption over a net 40 k.y. time period. Natural modern flux is from Pacyna and Pacyna (2001). Calculated increase in metal loading rates is based on metal/S ratio of Nriagu (1989) (mid-point of the range given was used) and total S flux of Siberian Trap volcanism (3.8×10^{13} Mg as SO_2) (Beerling et al., 2007).

Anoxia

Our study suggests that the main LPE horizon at Festningen occurs under oxic to dysoxic conditions, but that anoxia developed soon after and is associated with a final extinction of benthic life. There have been suggestions that the initial extinction event occurred under at least local, and perhaps regional, oxic conditions in other northwestern Pangean (Algeo et al., 2010; Knies et al., 2013; Proemse et al., 2013) and Neotethyan locations (Korte et al., 2004; Loope et al., 2013; Richoz et al., 2010). However, such conditions are commonly encountered only in shallower proximal settings. In the somewhat more distal setting of Tschermakfjellet, 60 km to the northwest of Festningen, the redox record indicates the gradual onset of oxygen-restricted deposition in the upper Kapp Starostin Formation (Dustira et al., 2013), whereas dysoxia is not seen in the shallower Festningen section until the latest Permian in the lower Vardebukta Formation. Similarly, in the Sverdrup Basin, Proemse et al. (2013) showed at the LPE a strongly developed oxygen minimum zone with euxinic conditions in deep-water settings and oxic shallow-water environments. This suggests a gradual expansion of dysoxic bottom waters into shallow-water environments (Grasby and Beauchamp, 2009; Proemse et al., 2013). It was during this expansion phase that the LPE occurred, even in locations like Festningen where oxic waters remained. As the habitable seafloor area shrank, the additional stress caused by intense trace metal poisoning may have driven the extinction of the low pH–tolerant benthos of northwestern Pangea. This relative timing of anoxia is consistent with paleo–marine temperature records that show that rapid warming of global oceans (which would drive enhanced anoxia) occurred after the main extinction event (Joachimski et al., 2012; Sun et al., 2012). This may imply then that the initial eruption of the Siberian Traps had an initial short-term toxic metal loading effect on global ecosystems that was followed by a delayed rapid global warming related to emissions of greenhouse gases (Dustira et al., 2013; Grasby and Beauchamp, 2009).

SUMMARY AND CONCLUSIONS

The Festningen section shows a remarkable record of progressive environmental deterioration through latest Permian time. Three major steps are observed, which we interpret as reflecting progressive ecological damage. First there was the gradual lysocline shoaling along the northwestern margin of Pangea leading to the final loss of carbonate producers at 12 m below the top of the Kapp Starostin Formation. Such loss of carbonate producers has been recorded over much of northwestern Pangea, where carbonate factories contracted into increasingly narrow mid- to inner shelf areas throughout the Middle Permian, and were nearly eradicated by Late Permian time except for in nearshore environments (Beauchamp and Grasby, 2012; Bugge et al., 1995; Ehrenberg et al., 2001; Gates et al., 2004). While these carbonate factories

were lost, silica productivity was maintained with the result that the nearshore siliceous limestones were replaced by across-the-shelf spiculites (Beauchamp and Baud, 2002; Beauchamp and Desrochers, 1997; Beauchamp and Grasby, 2012). This lysocline shoaling would reflect a gradual process related to long-term changes in atmospheric CO_2 that was most strongly manifest along the northwestern margin of Pangea in Late Permian time. However, such affects would not be expressed at low-latitude shelves in the Tethys that maintained productive carbonate factories.

Evidence for lysocline shoaling suggests that the Late Permian oceans were under progressive increasing stress on marine systems leading up to the LPE event. However, even if the loss of carbonate producers may reflect a progressive shift to a more stressed marine environment, siliceous sponges were able to still thrive, and diverse bioturbators continued to produce a pervasively burrowed fabric.

The second major environmental impact is recorded at the LPE event itself, when the loss of sponges and major loss of burrowing organisms occurred during oxic conditions. We argue that high metal loading rates at this time reflect onset of massive eruption of the Siberian Traps and associated volatile and toxic element release to the global atmosphere. Although burrowing animals still survived, trace fossils became limited to *Planolites* and small burrows (Wignall et al., 1998). Coincidental with the marine LPE, pollen records at this time indicate dramatic shifts to highly stressed terrestrial environments that imply simultaneous collapse of both marine and terrestrial systems.

The third major impact observed at Festningen is a distinct shift to anoxia 2.6 m above the LPE horizon associated with a distinct loss of remaining burrowers. We suggest that development of anoxia provided the third and final blow to the survivors. The continued spread of anoxia could have had several causes. Rapid increasing sea temperatures occurred just after the main extinction that would have decreased oxygen solubility (Romano et al., 2013; Sun et al., 2012) and could have also driven release of any remaining deep-marine gas hydrates, which would also have consumed dissolved oxygen in marine waters (Majorowicz, et al., 2014; Ruppel, 2011).

Results from this study show a remarkable record of environmental deterioration associated with the LPE event that struck progressively down ecologic systems, and demonstrates the need for high-resolution studies to characterize the nature of rapid change in global biogeochemical cycles during this dramatic period of Earth history.

ACKNOWLEDGMENTS

The Norwegian Polar Institute provided logistical support. Scanning electron microscope imaging was carried out in the Centre for Microscopy and Microanalysis at the University of Western Australia, which is funded by the university and the Western Australian and Australian governments. Zircon analyses were conducted using the SHRIMP II ion microprobe of the John de Laeter Centre for Isotope Research at Curtin University, Perth, Australia, operated by a Western Australia university-government consortium with ARC support. Reviews by Lee Kump and Matthew Clapham are greatly appreciated. This research was made possible by the Bundesanstalt für Geowissenschaftern und Rohstoffe, Geozentrum, the Natural Science and Engineering Research Council of Canada, and the Geological Survey of Canada (contribution 20140341).

REFERENCES CITED

Ader, M., Boudou, J.-P., Javoy, M., Goffe, B., and Daniels, E., 1998, Isotope study on organic nitrogen of Westphalian anthracites from the Western Middle field of Pennsylvania (U.S.A.) and from the Bramsche Massif (Germany): Organic Geochemistry, v. 29, p. 315–323, doi:10.1016/S0146-6380(98)00072-2.

Algeo, T.J., Hinnov, L., Moser, J., Maynard, J.B., Elswick, E., Kuwahara, K., and Sano, H., 2010, Changes in productivity and redox conditions in the Panthalassic Ocean during the latest Permian: Geology, v. 38, p. 187–190, doi:10.1130/G30483.1.

Algeo, T., Henderson, C.M., Ellwood, B., Rowe, H., Elswick, E., Bates, S., Lyons, T., Hower, J.C., Smith, C., Maynard, B., Hays, L.E., Summons, R.E., Fulton, J., and Freeman, K.H., 2012, Evidence for a diachronous Late Permian marine crisis from the Canadian Arctic region: Geological Society of America Bulletin, v. 124, p. 1424–1448., doi:10.1130/B30505.1.

Bagnato, E., Aiuppa, A., Bertagnini, A., Bonadonna, C., Cioni, R., Pistolesi, M., Pedone, M., and Hoskuldsson, A., 2013, Scavenging of sulphur, halogens and trace metals by volcanic ash: The 2010 Eyjafjallajökull eruption: Geochimica et Cosmochimica Acta, v. 103, p. 138–160, doi:10.1016/j.gca.2012.10.048.

Beauchamp, B., and Baud, A., 2002, Growth and demise of Permian biogenic chert along Northwest Pangea: Evidence for end-Permian collapse of thermohaline circulation: Palaeogeography, Palaeoclimatology, Palaeoecology, v. 184, p. 37–63, doi:10.1016/S0031-0182(02)00245-6.

Beauchamp, B., and Desrochers, A., 1997, Permian warm-to very cold-water carbonates and cherts in northwest Pangea, *in* James, N.P., and Clarke, J., eds., Cool-Water Carbonates: SEPM (Society for Sedimentary Geology) Special Publication 56, p. 327–347.

Beauchamp, B., and Grasby, S.E., 2012, Permian lysocline shoaling and ocean acidification along NW Pangea led to carbonate eradication and chert expansion: Palaeogeography, Palaeoclimatology, Palaeoecology, v. 350–352, p. 73–90, doi:10.1016/j.palaeo.2012.06.014.

Beauchamp, B., Henderson, C.M.B., Grasby, S.E., Gates, L., Beatty, T., Utting, J., and James, N.P., 2009, Late Permian sedimentation in the Sverdrup Basin, Canadian Arctic: The Lindström and Black Stripe formations: Canadian Society of Petroleum Geology Bulletin, v. 57, p. 167–191, doi:10.2113/gscpgbull.57.2.167.

Bebout, G.E., and Fogel, M.L., 1992, Nitrogen-isotope compositions of metasedimentary rocks in the Catalina Schist, California: Implications for metamorphic devolatilization history: Geochimica et Cosmochimica Acta, v. 56, p. 2839–2849, doi:10.1016/0016-7037(92)90363-N.

Bednar, A.J., Chappell, M.A., Seiter, J.M., Stanley, J.K., Averett, D.E., Jones, W.T., Pettway, B.A., Kennedy, A.J., Hendrix, S.H., and Steevens, J.A., 2010, Geochemical investigations of metals release from submerged coal fly ash using extended elutriate tests: Chemosphere, v. 81, p. 1393–1400, doi:10.1016/j.chemosphere.2010.09.026.

Beerling, D.J., Harfoot, M., Lomax, B., and Pyle, J.A., 2007, The stability of the stratospheric ozone layer during the end-Permian eruption of the Siberian Traps: Philosophical Transactions of the Royal Society of London A, v. 365, p. 1843–1866.

Berner, R.A., 2006, Inclusion of the weathering of volcanic rocks in the GEOCARBSULF model: American Journal of Science, v. 306, p. 295–302, doi:10.2475/05.2006.01.

Black, B.A., Elkins-Tanton, L.T., Rowe, M.C., and Peate, I.U., 2012, Magnitude and consequences of volatile release from the Siberian Traps: Earth and Planetary Science Letters, v. 317–318, p. 363–373, doi:10.1016/j.epsl.2011.12.001.

Black, B.A., Lamarque, J.-F., Shields, C.A., Elkins-Tanton, L.T., and Kiehl, J.T., 2014, Acid rain and ozone depletion from pulsed Siberian Traps magmatism: Geology, v. 42, p. 67–70, doi:10.1130/G34875.1.

Blinova, I., Bityukova, L., Kasemets, K., Ivask, A., Käkinen, A., Kurvet, I., Bondarenko, O., Kanarbik, L., Sihtmäe, M., Aruoja, V., Schvede, H., and Kahru, A., 2012, Environmental hazard of oil shale combustion fly ash: Journal of Hazardous Materials, v. 229–230, p. 192–200, doi:10.1016/j.jhazmat.2012.05.095.

Blomeier, D., Dustira, A.M., Forke, H., and Scheibner, C., 2013, Facies analysis and depositional environments of a storm-dominated, temperate to cold, mixed siliceous-carbonate ramp: The Permian Kapp Starostin Formation in NE Svalbard: Norwegian Journal of Geology, v. 93, p. 75–98.

Bond, D.P.G., and Wignall, P.B., 2010, Pyrite framboid study of marine Permian–Triassic boundary sections: A complex anoxic event and its relationship to contemporaneous mass extinction: Geological Society of America Bulletin, v. 122, p. 1265–1279, doi:10.1130/B30042.1.

Boyd, P.W., Watson, A.J., Law, C.S., Abraham, E.R., Trull, T., Murdoch, R., Bakker, D.C.E., Bowie, A.R., Buesseler, K.O., Chang, H., Charette, M., Croot, P., Downing, K., Frew, R., Gall, M., Hadfield, M., Hall, J., Harvey, M., Jameson, G., LaRoche, J., Liddicoat, M., Ling, R., Maldonado, M.T., McKay, R.M., Nodder, S., Pickmere, S., Pridmore, R., Rintoul, S., Safi, K., Sutton, P., Strzepek, R., Tanneberger, K., Turner, S., Waite, A., and Zeldis, J., 2000, A mesoscale phytoplankton bloom in the polar Southern Ocean stimulated by iron fertilization: Nature, v. 407, p. 695–702, doi:10.1038/35037500.

Bugge, T., Mangerud, G., Elvebakk, G., Mørk, A., Nilsson, I., Fanavoll, S., and Vigran, J.O., 1995, The Upper Paleozoic succession on the Finnmark Platform, Barents Sea: Norsk Geologisk Tidsskrift, v. 75, p. 3–30.

Burgess, S.D., Bowring, S., and Shen, S.-z., 2014, High-precision timeline for Earth's most severe extinction: Proceedings of the National Academy of Sciences of the United States of America, v. 111, p. 3316–3321, doi:10.1073/pnas.1317692111.

Campbell, I.H., Czamanske, G.K., Fedorenko, V.A., Hill, R.I., and Stepanov, V., 1992, Synchronism of the Siberian Traps and the Permian-Triassic boundary: Science, v. 258, p. 1760–1763, doi:10.1126/science.258.5089.1760.

CASE (Circum-Arctic Structural Events) Team, 2001, The evolution of the West Spitsbergen Fold-and-Thrust Belt, *in* Tessensohn, F., ed., Intra-Continental Fold Belts: CASE 1: West Spitsbergen: Geologisches Jahrbuch, v. B91, p. 733–773.

Compston, W., Williams, I.S., and Meyer, C., 1984, U-Pb geochronology of zircons from lunar breccia 73217 using a sensitive high mass-resolution ion microprobe: Journal of Geophysical Research, v. 89, p. 525–534, doi:10.1029/JB089iS02p0B525.

Corfu, F., Polteau, S., Planke, S., Faleide, J.I., Svensen, H., Zayoncheck, A., and Stolbov, N., 2013, U–Pb geochronology of Cretaceous magmatism on Svalbard and Franz Josef Land, Barents Sea Large Igneous Province: Geological Magazine, v. 150, p. 1127–1135, doi:10.1017/S0016756813000162.

Courtillot, V., Jaupart, C., Manighetti, I., Tapponnier, P., and Besse, J., 1999, On causal links between flood basalts

and continental breakup: Earth and Planetary Science Letters, v. 166, p. 177–195, doi:10.1016/S0012-821X(98)00282-9.

Cui, Y., and Kump, L.R., 2014, Global warming and the end-Permian extinction event: Proxy and modeling perspectives: Earth-Science Reviews, doi:10.1016/j.earscirev.2014.04.007 (in press).

Dallmann, W., Andresen, A., Bergh, S.G., Maher, H.D., and Otha, Y., 1993, Tertiary fold-and-thrust belt of Spitsbergen, Svalbard: Norsk Polarinstitute Meddelelser, v. 128, p. 1–46.

Davison, R.L., Natusch, D.F.S., Wallace, J.R., and Evans, C.A., 1974, Trace elements in fly ash: Dependence of concentration on particle size: Environmental Science & Technology, v. 8, p. 1107–1113, doi:10.1021/es60098a003.

Dustira, A.M., Wignall, P.B., Joachimski, M., Blomeier, D., Hartkopf-Fröder, C., and Bond, D.P.G., 2013, Gradual onset of anoxia across the Permian–Triassic Boundary in Svalbard, Norway: Palaeogeography, Palaeoclimatology, Palaeoecology, v. 374, p. 303–313, doi:10.1016/j.palaeo.2013.02.004.

Ehrenberg, S.N., Pickard, N.A.H., Henriksen, L.B., Svånå, T.A., Gutteridge, P., and Macdonald, D., 2001, A depositional and sequence stratigraphic model for cold-water, spiculitic strata based on the Kapp Starostin Formation (Permian) of Spitsbergen and equivalent deposits from the Barents Sea: AAPG Bulletin, v. 85, p. 2061–2087.

Embry, A.F., 1992, Crockerland: The northwest source area for the Sverdrup Basin, Canadian Arctic Islands, *in* Vorren, T.O., Bergsager, E., Dahl-Stamnes, Ø.A., Holter, E., Johansen, B., Lie, E., and Lund, T.B., eds., Arctic Geology and Petroleum Potential, Volume 2: Amsterdam, Elsevier, p. 205–216.

Embry, A.F., and Beauchamp, B., 2008, Sverdrup Basin, *in* Miall, A.D., ed., The Sedimentary Basins of Unites States and Canada: Amsterdam, Elsevier, p. 451–472.

Erwin, D.H., 2006, Extinction: How Life on Earth Nearly Ended 250 Million Years Ago: New Jersey, Princeton University Press.

Fedo, C.M., Nesbitt, H.W., and Young, G.M., 1995, Unraveling the effects of potassium metasomatism in sedimentary rocks and paleosols, with implications for paleoweathering conditions and provenance: Geology, v. 23, p. 921–924, doi:10.1130/0091-7613(1995)023<0921:UTEOPM>2.3.CO;2.

Fedorenko, V., Czamanske, G., Zen'ko, T., Budahn, J., and Siems, D., 2000, Field and geochemical studies of the melilite-bearing Arydzhangsky Suite, and an overall perspective on the Siberian alkaline-ultramafic flood-volcanic rocks: International Geology Review, v. 42, p. 769–804, doi:10.1080/00206810009465111.

Frogner Kockum, P.C., Herbert, R.B., and Gislason, S.R., 2006, A diverse ecosystem response to volcanic aerosols: Chemical Geology, v. 231, p. 57–66, doi:10.1016/j.chemgeo.2005.12.008.

Furuya, K., Miyajima, Y., Chiba, T., and Kikuchi, T., 1987, Elemental characterization of particle size-density separated coal fly ash by spectrophotometry, ICP (inductively coupled plasma emission spectrometry), and scanning electron microscopy-energy dispersive x-ray analysis: Environmental Science & Technology, v. 21, p. 898–903, doi:10.1021/es00163a008.

Gates, L., James, N.P., and Beauchamp, B., 2004, A glass ramp: Shallow-water Permian spiculitic chert sedimentation, Sverdrup Basin, Arctic Canada: Sedimentary Geology, v. 168, p. 125–147, doi:10.1016/j.sedgeo.2004.03.008.

Gieré, R., Carleton, L.E., and Lumpkin, G.R., 2003, Micro- and nanochemistry of fly ash from a coal-fired power plant: The American Mineralogist, v. 88, p. 1853–1865.

Golonka, J., and Ford, D., 2000, Pangean (Late Carboniferous–Middle Jurassic) paleoenvironment and lithofacies: Palaeogeography, Palaeoclimatology, Palaeoecology, v. 161, p. 1–34, doi:10.1016/S0031-0182(00)00115-2.

Grasby, S.E., and Beauchamp, B., 2008, Intrabasin variability of the carbon-isotope record across the Permian-Triassic transition, Sverdrup Basin, Arctic Canada: Chemical Geology, v. 253, p. 141–150, doi:10.1016/j.chemgeo.2008.05.005.

Grasby, S.E., and Beauchamp, B., 2009, Latest Permian to Early Triassic basin-to-shelf anoxia in the Sverdrup Basin, Arctic Canada: Chemical Geology, v. 264, p. 232–246, doi:10.1016/j.chemgeo.2009.03.009.

Grasby, S.E., Sanei, H., and Beauchamp, B., 2011, Catastrophic dispersion of coal fly ash into oceans during the latest Permian extinction: Nature Geoscience, v. 4, p. 104–107, doi:10.1038/ngeo1069.

Grasby, S.E., Beauchamp, B., Embry, A.F., and Sanei, H., 2013a, Recurrent Early Triassic ocean anoxia: Geology, v. 41, p. 175–178, doi:10.1130/G33599.1.

Grasby, S.E., Sanei, H., Beauchamp, B., and Chen, Z., 2013b, Mercury deposition through the Permo–Triassic Biotic Crisis: Chemical Geology, v. 351, p. 209–216, doi:10.1016/j.chemgeo.2013.05.022.

Grice, K., Cao, C., Love, G.D., Böttcher, M.E., Twitchett, R.J., Grosjean, E., Summons, R.E., Turgeon, S.C., Dunning, W., and Jin, Y., 2005, Photic zone euxinia during the Permian-Triassic superanoxic event: Science, v. 307, p. 706–709, doi:10.1126/science.1104323.

Hall, G., and Pelchat, P., 1997, Evaluation of a direct solid sampling atomic absorption spectrometer for the trace determination of mercury in geological samples: Analyst (London), v. 122, p. 921–924, doi:10.1039/a700194k.

Hayes, J.M., Kaplan, I.R., and Wedeking, K.W., 1983, *in* Schopf, J.W., ed., Earth's Earliest Biosphere: Its Origin and Evolution: Princeton NJ, Princeton University Press, p. 92–132.

Hays, L., Beatty, T., Henderson, C.M.B., Love, G.D., and Summons, R.E., 2007, Evidence for photic zone euxinia through the end-Permian mass extinction in the Panthalassic Ocean (Peace River Basin, Western Canada): Palaeoworld, v. 16, p. 39–50, doi:10.1016/j.palwor.2007.05.008.

Hellman, F.J., Gee, D.G., and Witt-Nilsson, P., 2001, Late Archean basement in the Bangenhuken Complex of the Nordbreen Nappe, western Ny-Friesland, Svalbard: Polar Research, v. 20, p. 49–59, doi:10.1111/j.1751-8369.2001.tb00038.x.

Henderson, C.M., and Baud, A., 1997, Correlation of the Permian-Triassic boundary in Arctic Canada and comparison with Meishan, China, *in* Wang, N., and Remane, J., eds., Proceedings of the 30th International Geological Congress, Volume 11: Stratigraphy: Utrecht, VSP, p. 143–152.

Hermann, E., Hochuli, P.A., Bucher, H., Vigran, J.O., Weissert, H., and Bernasconi, S.M., 2010, A close-up view of the Permian–Triassic boundary based on expanded organic carbon isotope records from Norway (Trøndelag and Finnmark Platform): Global and Planetary Change, v. 74, p. 156–167, doi:10.1016/j.gloplacha.2010.10.007.

Heydari, E., and Hassanzadeh, J., 2003, Deev Jahi Model of the Permian-Triassic boundary mass extinction: A case for gas hydrates as the main cause of biological crisis on Earth: Sedimentary Geology, v. 163, p. 147–163, doi:10.1016/j.sedgeo.2003.08.002.

Hochuli, P.A., Hermann, E., Vigran, J.O., Bucher, H., and Weissert, H., 2010, Rapid demise and recovery of plant ecosystems across the end-Permian extinction event: Global and Planetary Change, v. 74, p. 144–155, doi:10.1016/j.gloplacha.2010.10.004.

Hoffmann, L.J., Breitbarth, E., Ardelan, M.V., Duggen, S., Olgun, N., Hassellöv, M., and Wängberg, S.Å., 2012, Influence of trace metal release from volcanic ash on growth of *Thalassiosira pseudonana* and *Emiliania huxleyi*: Marine Chemistry, v. 132–133, p. 28–33, doi:10.1016/j.marchem.2012.02.003.

Isozaki, Y., 1997, Permo-Triassic boundary superanoxia and stratified superocean: Records from lost deep sea: Science, v. 276, p. 235–238, doi:10.1126/science.276.5310.235.

Joachimski, M.M., Lai, X., Shen, S., Jiang, H., Luo, G., Chen, B., Chen, J., and Sun, Y., 2012, Climate warming in the latest Permian and the Permian–Triassic mass extinction: Geology, v. 40, p. 195–198, doi:10.1130/G32707.1.

Johansson, Å., Larionov, A.N., Tebenkov, A.M., Ohta, Y., and Gee, D.G., 2002, Caledonian granites of western and central Nordaustlandet, northeast Svalbard: GFF (Journal of the Geological Society of Sweden), v. 124, p. 135–148, doi:10.1080/11035890201243135.

Jones, M.T., and Gislason, S.R., 2008, Rapid releases of metal salts and nutrients following the deposition of volcanic ash into aqueous environments: Geochimica et Cosmochimica Acta, v. 72, p. 3661–3680, doi:10.1016/j.gca.2008.05.030.

Kaakinen, J.W., Jorden, R.M., Lawasani, M.H., and West, R.E., 1975, Trace element behavior in coal-fired power plant: Environmental Science & Technology, v. 9, p. 862–869, doi:10.1021/es60107a012.

Kaiho, K., and Koga, S., 2013, Impacts of a massive release of methane and hydrogen sulfide on oxygen and ozone during the late Permian mass extinction: Global and Planetary Change, v. 107, p. 91–101, doi:10.1016/j.gloplacha.2013.04.004.

Kaiho, K., Kajiwara, Y., Nakano, T., Miura, Y., Kawahata, H., Tazaki, K., Ueshima, M., Chen, Z., and Shi, G.R., 2001, End-Permian catastrophe by a bolide impact: Evidence of a gigantic release of sulfur from the mantle: Geology, v. 29, p. 815–818, doi:10.1130/0091-7613(2001)029<0815:EPCBAB>2.0.CO;2.

Kidder, D.L., and Worsley, T.R., 2004, Causes and consequences of extreme Permo-Triassic warming to globally equable climate and relation to the Permo-Triassic extinction and recovery: Palaeogeography, Palaeoclimatology, Palaeoecology, v. 203, p. 207–237, doi:10.1016/S0031-0182(03)00667-9.

Kidder, D.L., and Worsley, T.R., 2010, Phanerozoic Large Igneous Provinces (LIPs), HEATT (Haline Euxinic Acidic Thermal Transgression) episodes, and mass extinctions: Palaeogeography, Palaeoclimatology, Palaeoecology, v. 295, p. 162–191, doi:10.1016/j.palaeo.2010.05.036.

Klein, D.H., Andren, A.W., Carter, J.A., Emery, J.F., Feldman, C., Fulkerson, W., Lyon, W.S., Ogle, J.C., and Talmi, Y., 1975, Pathways of thirty-seven trace elements through coal-fired power plant: Environmental Science & Technology, v. 9, p. 973–979, doi:10.1021/es60108a007.

Knies, J., Grasby, S.E., Beauchamp, B., and Schubert, C., 2013, Water mass denitrification during the latest Permian extinction in the Sverdrup Basin, Arctic Canada: Geology, v. 41, p. 167–170, doi:10.1130/G33816.1.

Knoll, A.H., Bambach, R.K., Canfield, D.E., and Grotzinger, J.P., 1996, Comparative Earth history and Late Permian mass extinction: Science, v. 273, p. 452–457, doi:10.1126/science.273.5274.452.

Konhauser, K.O., Pecoits, E., Lalonde, S.V., Papineau, D., Nisbet, E.G., Barley, M.E., Arndt, N.T., Zahnle, K., and Kamber, B.S., 2009, Oceanic nickel depletion and a methanogen famine before the Great Oxidation Event: Nature, v. 458, p. 750–753, doi:10.1038/nature07858.

Korte, C., and Kozur, H.W., 2010, Carbon-isotope stratigraphy across the Permian-Triassic boundary: A review: Journal of Asian Earth Sciences, v. 39, p. 215–235, doi:10.1016/j.jseaes.2010.01.005.

Korte, C., Kozur, H.W., and Partoazar, H., 2004, Negative carbon isotope excursion at the Permian/Triassic boundary section at Zal, NW-Iran: Hallesches Jahrbuch für Geowissenschaften B, v. 18, p. 69–71.

Korte, C., Pande, P., Kalia, P., Kozur, H.W., Joachimski, M.M., and Oberhansli, H., 2010, Massive volcanism at the Permian-Triassic boundary and its impact on the isotopic composition of the ocean and atmosphere: Journal of Asian Earth Sciences, v. 37, p. 293–311, doi:10.1016/j.jseaes.2009.08.012.

Kump, L.R., Pavlov, A., and Arthur, M.A., 2005, Massive release of hydrogen sulfide to the surface ocean and atmosphere during intervals of oceanic anoxia: Geology, v. 33, p. 397–400, doi:10.1130/G21295.1.

Lafargue, E., Espitalité, J., Marquis, F., and Pillot, D., 1998, Rock-Eval 6 applications in hydrocarbon exploration, production, and soil contamination studies: Revue de l'Institut Français du Pétrole, v. 53, p. 421–437, doi:10.2516/ogst:1998036.

Langmann, B., Zaksek, K., Hort, M., and Duggen, S., 2010, Volcanic ash as fertiliser for the surface ocean: Atmospheric Chemistry and Physics, v. 10, p. 3891–3899, doi:10.5194/acp-10-3891-2010.

Lehrmann, D.J., 1999, Early Triassic calcimicrobial mounds and biostromes of Nanpanjiang basin, south China: Geology, v. 27, p. 359–362, doi:10.1130/0091-7613(1999)027<0359:ETCMAB>2.3.CO;2.

Liang, H., 2002, End-Permian catastrophic event of marine acidification by hydrated sulfuric acid: Mineralogical evidence from Meishan Section of South China: Chinese Science Bulletin, v. 47, p. 1393–1397, doi:10.1360/02tb9307.

Loope, G.R., Kump, L.R., and Arthur, M.A., 2013, Shallow water redox conditions from the Permian–Triassic boundary microbialite: The rare earth element and iodine geochemistry of carbonates from Turkey and South China: Chemical Geology, v. 351, p. 195–208, doi:10.1016/j.chemgeo.2013.05.014.

Ludwig, K.R., 2003, Isoplot 3.0: A geochronological toolkit for Microsoft Excel: Berkeley Geochronology Center Special Publication 4, 70 p.

Ludwig, K.R., 2009, SQUID 2 (rev. 2.50): A user's manual: Berkeley Geochronology Center Special Publication 5, 95 p.

Maher, H.D., and Craddock, C., 1988, Decoupling as an alternate model for transpression during the initial opening of the Norwegian Greenland Sea: Polar Research, v. 6, p. 137–140.

Majorowicz, J., Grasby, S.E., Safanda, J., and Beauchamp, B., 2014, Gas hydrate contribution to Late Permian global warming: Earth and Planetary Science Letters, v. 393, p. 243–253.

Mangerud, G., and Konieczny, R.M., 1993, Palynology of the Permian succession of Spitsbergen, Svalbard: Polar Research, v. 12, p. 65–93, doi:10.1111/j.1751-8369.1993.tb00423.x.

Martin, R.E., 1996, Secular increase in nutrient levels throughout the Phanerozoic: Implications for productivity, biomass, and diversity of the marine biosphere: Palaios, v. 11, p. 209–219, doi:10.2307/3515230.

Martinez-Tarazona, M.R., and Spears, D.A., 1996, The fate of trace elements and bulk minerals in pulverized coal combustion in a power station: Fuel Processing Technology, v. 47, p. 79–92, doi:10.1016/0378-3820(96)01001-6.

Mather, T.A., Pyle, D.M., and Oppenheimer, C., 2013, Tropospheric volcanic aerosol, *in* Robock, A., and Oppenheimer, C., eds., Volcanism and the Earth's Atmosphere: American Geophysical Union Geophysical Monograph 139, p. 189–212.

Mørk, A., Knarud, R., and Worsley, D., 1982, Depositional and diagenetic environments of the Triassic and Lower Jurassic succession of Svalbard, *in* Embry, A.F., and Balkwill, H.R., eds., Arctic Geology and Geophysics: Proceedings of the Third International Symposium on Arctic Geology: Calgary, Canadian Society of Petroleum Geologists, p. 371–398.

Nakamura, K., Kimura, G., and Winsnes, T.S., 1987, Brachiopod zonation and age of the Permian Kapp Starostin Formation (central Spitsbergen): Polar Research, v. 5, p. 207–219, doi:10.1111/j.1751-8369.1987.tb00623.x.

Nakrem, H.A., Orchard, M.J., Weitschat, W., Hounslow, M.W., Beatty, T.W., and Mørk, A., 2008, Triassic conodonts from Svalbard and their Boreal correlations: Polar Research, v. 27, p. 523–539, doi:10.1111/j.1751-8369.2008.00076.x.

Nesbitt, H.W., and Young, G.M., 1982, Early Proterozoic climates and plate motions inferred from major element chemistry of lutites: Nature, v. 299, p. 715–717, doi:10.1038/299715a0.

Nriagu, J.O., 1989, A global assessment of natural sources of atmospheric trace metals: Nature, v. 338, p. 47–49, doi:10.1038/338047a0.

Odasz-Albrigtsen, A.M., Tømmervik, H., and Murphy, P., 2000, Decreased photosynthetic efficiency in plant species exposed to multiple airborne pollutants along the Russian-Norwegian border: Canadian Journal of Botany, v. 78, p. 1021–1033, doi:10.1139/b00-075.

Ogden, D.E., and Sleep, N.H., 2012, Explosive eruption of coal and basalt and the end-Permian mass extinction: Proceedings of the National Academy of Sciences of the United States of America, v. 109, p. 59–62, doi:10.1073/pnas.1118675109.

Olsson, J., Stipp, S.L.S., Dalby, K.N., and Gislason, S.R., 2013, Rapid release of metal salts and nutrients from the 2011 Grímsvötn, Iceland volcanic ash: Geochimica et Cosmochimica Acta, v. 123, p. 134–149, doi:10.1016/j.gca.2013.09.009.

Pacyna, J.M., and Pacyna, E.G., 2001, An assessment of global and regional emissions of trace metals to the atmosphere from anthropogenic sources worldwide: Environmental Reviews, v. 9, p. 269–298, doi:10.1139/a01-012.

Papastefanou, C., 2010, Escaping radioactivity from coal-fired power plants (CPPs) due to coal burning and the associated hazards: A review: Journal of Environmental Radioactivity, v. 101, p. 191–200, doi:10.1016/j.jenvrad.2009.11.006.

Pavlov, V.E., Fluteau, F., Veselovskiy, R.V., Fetisova, A.M., and Latyshev, A.V., 2011, Secular geomagnetic variations and volcanic pulses in the Permian-Triassic traps of the Norilsk and Maimecha-Kotui provinces: Izvestiya, Physics of the Solid Earth, v. 47, p. 402–417, doi:10.1134/S1069351311040070.

Payne, J.L., and van de Schootbrugge, B., 2007, Life in Triassic oceans: Links between planktonic and benthic recovery and radiation, *in* Falkowski, P.G., and Knoll, A.H., eds., Evolution of Primary Producers in the Sea: Amsterdam, Academic Press, p. 165–189.

Payne, J.L., Lehrmann, D.J., Follett, D., Seibel, M., Kump, L.R., Riccardi, A., Altiner, D., Sano, H., and Wei, J., 2007, Erosional truncation of uppermost Permian shallow-marine carbonates and implications for Permian-Triassic boundary events: Geological Society of America Bulletin, v. 119, p. 771–784, doi:10.1130/B26091.1.

Proemse, B.C., Grasby, S.E., Wieser, M.E., Mayer, B., and Beauchamp, B., 2013, Molybdenum isotopic evidence for oxic marine conditions during the latest Permian extinction: Geology, v. 41, p. 967–970, doi:10.1130/G34466.1.

Pyle, D.M., and Mather, T.A., 2003, The importance of volcanic emissions for the global atmospheric mercury cycle: Atmospheric Environment, v. 37, p. 5115–5124, doi:10.1016/j.atmosenv.2003.07.011.

Raiswell, R., and Berner, R.A., 1985, Pyrite formation in euxinic and semi-euxinic sediments: American Journal of Science, v. 285, p. 710–724, doi:10.2475/ajs.285.8.710.

Reichow, M.K., Pringle, M.S., Al'Mukhamedov, A.I., Allen, M.B., Andreichev, V.L., Buslov, M.M., Davies, C.E., Fedoseev, G.S., Fitton, J.G., Inger, S., Medvedev, A.Y., Mitchell, C., Puchkov, V.N., Safonova, I.Y., Scott, R.A., and Saunders, A.D., 2009, The timing and extent of the eruption of the Siberian Traps large igneous province: Implications for the end-Permian environmental crisis: Earth and Planetary Science Letters, v. 277, p. 9–20, doi:10.1016/j.epsl.2008.09.030.

Reid, C.M., James, N.P., Beauchamp, B., and Kyser, T.K., 2007, Faunal turnover and changing oceanography: Late Palaeozoic warm-to-cool water carbonates, Sverdrup Basin, Canadian Arctic Archipelago: Palaeogeography, Palaeoclimatology: Palaeoecology, v. 249, p. 128–159, doi:10.1016/j.palaeo.2007.01.007.

Renne, P.R., Black, M.T., Zichao, Z., Richards, M.A., and Basu, A.R., 1995, Synchrony and causal relations between Permian-Triassic boundary crises and Siberian flood volcanism: Science, v. 269, p. 1413–1416, doi:10.1126/science.269.5229.1413.

Retallack, G.J., 1999, Postapocalyptic greenhouse paleoclimate revealed by earliest Triassic paleosols in the Sydney Basin, Australia: Geological Society of America Bulletin, v. 111, p. 52–70, doi:10.1130/0016-7606(1999)111<0052:PGPRBE>2.3.CO;2.

Retallack, G.J., and Jahren, A.H., 2008, Methane release from igneous intrusion of coal during Late Permian extinction events: The Journal of Geology, v. 116, p. 1–20, doi:10.1086/524120.

Retallack, G.J., and Krull, E.S., 2006, Carbon isotopic evidence for terminal-Permian methane outbursts and their role in extinctions of animals, plants, coral reefs, and peat swamps, *in* Greb, S.F., and DiMichele, W.A., eds., Wetlands Through Time: Geological Society of America Special Paper 399, p. 249–268.

Richoz, S., Krystyn, L., Baud, A., Brandner, R., Horacek, M., and Mohtat-Aghai, P., 2010, Permian–Triassic boundary interval in the Middle East (Iran and N. Oman): Progressive environmental change from detailed carbonate carbon isotope marine curve and sedimentary evolution: Journal of Asian Earth Sciences, v. 39, p. 236–253, doi:10.1016/j.jseaes.2009.12.014.

Romano, C., Goudemand, N., Vennemann, T.W., Ware, D., Schneebeli-Hermann, E., Hochuli, P.A., Bruhwiler, T., Brinkmann, W., and Bucher, H., 2013, Climatic and biotic upheavals following the end-Permian mass extinction: Nature Geoscience, v. 6, p. 57–60, doi:10.1038/ngeo1667.

Rothman, D.H., Fournier, G.P., French, K.L., Alm, E.J., Boyle, E.A., Cao, C., and Summons, R.E., 2014, Methanogenic burst in the end-Permian carbon cycle: Proceedings of the National Academy of Sciences of the United States of America, v. 111, p. 5462–5467, doi:10.1073/pnas.1318106111.

Ruggieri, F., Fernández-Turiel, J.-L., Saavedra, J., Gimeno, D., Polanco, E., and Naranjo, J.A., 2011, Environmental geochemistry of recent volcanic ashes from the Southern Andes: Environmental Chemistry, v. 8, p. 236–247, doi:10.1071/EN10097.

Ruppel, C.D., 2011, Methane Hydrates and Contemporary Climate Change: Nature Education Knowledge v. 2, p. 12.

Sanei, H., Grasby, S.E., and Beauchamp, B., 2012, Latest Permian mercury anomalies: Geology, v. 40, p. 63–66, doi:10.1130/G32596.1.

Saunders, A.D., and Reichow, M.K., 2009, The Siberian Traps and the End-Permian mass extinction: A critical review: Chinese Science Bulletin, v. 54, p. 20–37, doi:10.1007/s11434-008-0543-7.

Schoepfer, S.D., Henderson, C.M., Garrison, G.H., Foriel, J., Ward, P.D., Selby, D., Hower, J.C., Algeo, T.J., and Shen, Y., 2013, Termination of a continent-margin upwelling system at the Permian–Triassic boundary (Opal Creek, Alberta, Canada): Global and Planetary Change, v. 105, p. 21–35, doi:10.1016/j.gloplacha.2012.07.005.

Scotese, C.R., 2004, A continental drift flipbook: The Journal of Geology, v. 112, p. 729–741, doi:10.1086/424867.

Scott, C., and Lyons, T.W., 2012, Contrasting molybdenum cycling and isotopic properties in euxinic versus non-euxinic sediments and sedimentary rocks: Refining the paleoproxies: Chemical Geology, v. 324–325, p. 19–27, doi:10.1016/j.chemgeo.2012.05.012.

Sephton, M.A., Looy, C.V., Brinkhuis, H., Wignall, P.B., de Leeuw, J.W., and Visscher, H., 2005, Catastrophic soil erosion during the end-Permian biotic crisis: Geology, v. 33, p. 941–944, doi:10.1130/G21784.1.

Sephton, M.A., Jiao, D., Engel, M.H., Looy, C.V., and Visscher, H., 2015, Terrestrial acidification during the end-Permian biosphere crisis?: Geology, doi:10.1130/G36227.1.

Sheldon, N.D., 2006, Abrupt chemical weathering increase across the Permian-Triassic boundary: Palaeogeography, Palaeoclimatology, Palaeoecology, v. 231, p. 315–321, doi:10.1016/j.palaeo.2005.09.001.

Shen, S.-z., Crowley, J.L., Wang, Y., Bowring, S.A., Erwin, D.H., Sadler, P.M., Cao, C.-q., Rothman, D.H., Henderson, C.M., Ramezani, J., Zhang, H., Shen, Y., Wang, X.-d., Wang, W., Mu, L., Li, W.-z., Tang, Y.-g., Liu, X.-l., Liu, L.-j., Zeng, Y., Jiang, Y.-f., and Jin, Y.-g., 2011, Calibrating the end-Permian mass extinction: Science, v. 334, p. 1367–1372, doi:10.1126/science.1213454.

Sial, A.N., Lacerda, L.D., Ferreira, V.P., Frei, R., Marquillas, R.A., Barbosa, J.A., Gaucher, C., Windmöller, C.C., and Pereira, N.S., 2013, Mercury as a proxy for volcanic activity during extreme environmental turnover: The Cretaceous–Paleogene transition: Palaeogeography, Palaeoclimatology, Palaeoecology, v. 387, p. 153–164, doi:10.1016/j.palaeo.2013.07.019.

Silva, M.V.N., Sial, A.N., Barbosa, J.A., Ferreira, V.P., Neumann, V.H., and De Lacerda, L.D., 2013, Carbon isotopes, rare-earth elements and mercury geochemistry across the K–T transition of the Paraíba Basin, northeastern Brazil, *in* Bojar, A.-V., Melinte-Dobrinescu, M.C., and Smit, J., eds., Isotopic Studies in Cretaceous Research: Geological Society of London Special Publication 382, p. 85–104, doi:10.1144/SP382.2.

Smith, R.D., Campbell, J.A., and Nielson, K.K., 1979, Concentration dependence upon particle size of volatilized

elements in fly ash: Environmental Science & Technology, v. 13, p. 553–558, doi:10.1021/es60153a003.

Song, H., Wignall, P.B., Chu, D., Tong, J., Sun, Y., Song, H., He, W., and Tian, L., 2014, Anoxia/high temperature double whammy during the Permian-Triassic marine crisis and its aftermath: Scientific Reports, v. 4, 4132, doi:10.1038/srep04132.

Stacey, J.S., and Kramers, J.D., 1975, Approximation of terrestrial lead isotope evolution by a two-stage model: Earth and Planetary Science Letters, v. 26, p. 207–221, doi:10.1016/0012-821X(75)90088-6.

Stemmerik, L., and Worsley, D., 1995, Permian history of the Barents Shelf area, *in* Scholle, P., Peryt, T., and Ulmer-Scholle, D., eds., The Permian of Northern Pangea: Berlin-Heidelberg, Springer, p. 81–97.

Stemmerik, L., and Worsley, D., 2005, 30 years on: Arctic Upper Palaeozoic stratigraphy, depositional evolution and hydrocarbon prospectivity: Norsk Geologisk Tidsskrift, v. 85, p. 151–168.

Stern, R.A., 2001, A new isotopic and trace-element standard for the ion microprobe: Preliminary thermal ionization mass spectrometry (TIMS) U-Pb and electron-microprobe data: Geological Survey of Canada Current Research 2001-F1, Radiogenic Age and Isotopic Studies Report 14, 7 p.

Stern, R.A., Bodorkos, S., Kamo, S.L., Hickman, A.H., and Corfu, F., 2009, Measurement of SIMS instrumental mass fractionation of Pb isotopes during zircon dating: Geostandards and Geoanalytical Research, v. 33, p. 145–168, doi:10.1111/j.1751-908X.2009.00023.x.

Sun, Y., Joachimski, M.M., Wignall, P.B., Yan, C., Chen, Y., Jiang, H., Wang, L., and Lai, X., 2012, Lethally hot temperatures during the Early Triassic greenhouse: Science, v. 338, p. 366–370, doi:10.1126/science.1224126.

Svensen, H., Planke, S., Polozov, A.G., Schmidbauer, N., Corfu, F., Podladchikov, Y.Y., and Jamtveit, B., 2009, Siberian gas venting and the end-Permian environmental crisis: Earth and Planetary Science Letters, v. 277, p. 490–500, doi:10.1016/j.epsl.2008.11.015.

Symonds, R.B., Rose, W.I., Reed, M.H., Lichte, F.E., and Finnegan, D.L., 1987, Volatilization, transport and sublimation of metallic and non-metallic elements in high temperature gases at Merapi Volcano, Indonesia: Geochimica et Cosmochimica Acta, v. 51, p. 2083–2101, doi:10.1016/0016-7037(87)90258-4.

Taylor, S.R., and McLennan, S.M., 1985, The Continental Crust: Its Composition and Evolution: Oxford, Blackwell, 312 p.

Tozer, E.T., and Parker, J.R., 1968, Notes on the Triassic biostratigraphy of Svalbard: Geological Magazine, v. 105, p. 526–542.

Tribovillard, N., Algeo, T.J., Lyons, T., and Riboulleau, A., 2006, Trace metals as paleoredox and paleoproductivity proxies: An update: Chemical Geology, v. 232, p. 12–32, doi:10.1016/j.chemgeo.2006.02.012.

Twitchett, R.J., Looy, C.V., Morante, R., Visscher, H., and Wignall, P.B., 2001, Rapid and synchronous collapse of marine and terrestrial ecosystems during the end-Permian biotic crisis: Geology, v. 29, p. 351–354, doi:10.1130/0091-7613(2001)029<0351:RASCOM>2.0.CO;2.

Vie le Sage, R., 1983, Chemistry of the volcanic aerosol, *in* Tazieff, H., and Sabroux, J.-C., eds., Forecasting Volcanic Events: Amsterdam, Elsevier, p. 445–474.

Wang, K., Geldsetzer, H.H.J., and Krouse, H.R., 1994, Permian-Triassic extinction: Organic $\delta^{13}C$ evidence from British Columbia, Canada: Geology, v. 22, p. 580–584, doi:10.1130/0091-7613(1994)022<0580:PTEOCE>2.3.CO;2.

Wedepohl, K.H., 1991, The composition of the continental crust: Geochimica et Cosmochimica Acta, v. 59, no. 7, p. 1217–1232.

White, R.V., and Saunders, A.D., 2005, Volcanism, impact and mass extinctions: Incredible or credible coincidences?: Lithos, v. 79, p. 299–316, doi:10.1016/j.lithos.2004.09.016.

Wignall, P.B., 2001, Large igneous provinces and mass extinctions: Earth-Science Reviews, v. 53, p. 1–33, doi:10.1016/S0012-8252(00)00037-4.

Wignall, P.B., and Hallam, A., 1992, Anoxia as a cause of the Permian/Triassic mass extinction: Facies evidence from northern Italy and the western United States: Palaeogeography, Palaeoclimatology, Palaeoecology, v. 93, p. 21–46, doi:10.1016/0031-0182(92)90182-5.

Wignall, P.B., and Newton, R., 2003, Contrasting deep-water records from the Upper Permian and Lower Triassic of South Tibet and British Columbia: Evidence for a diachronous mass extinction: Palaios, v. 18, p. 153–167, doi:10.1669/0883-1351(2003)18<153:CDRFTU>2.0.CO;2.

Wignall, P.B., and Twitchett, R.J., 1996, Oceanic anoxia and the end Permian mass extinction: Science, v. 272, p. 1155–1158, doi:10.1126/science.272.5265.1155.

Wignall, P.B., Morante, R., and Newton, R., 1998, The Permo-Triassic transition in Spitsbergen: $\delta^{13}C_{org}$ chemostratigraphy, Fe and S geochemistry, facies, fauna and trace fossils: Geological Magazine, v. 135, p. 47–62, doi:10.1017/S0016756897008121.

Williams, I.S., 1998, U-Th-Pb geochronology by ion microprobe, *in* McKibben, M.A., Shanks, W.C., and Ridely, W.I., eds., Applications of Microanalytical Techniques to Understanding Mineralizing Processes: Society of Economic Geologists, p. 1–35.

Xie, S., Pancost, R.D., Yin, H., Wang, H., and Evershed, R.P., 2005, Two episodes of microbial change coupled with Permo/Triassic faunal mass extinction: Nature, v. 434, p. 494–497, doi:10.1038/nature03396.

Xie, S., Pancost, R.D., Huang, J., Wignall, P.B., Yu, J., Tang, X., Chen, L., Huang, X., and Lai, X., 2007, Changes in the global carbon cycle occurred as two episodes during the Permian–Triassic crisis: Geology, v. 35, p. 1083–1086, doi:10.1130/G24224A.1.

Xie, S., Pancost, R.D., Wang, Y., Yang, H., Wignall, P.B., Luo, G., Jia, C., and Chen, L., 2010, Cyanobacterial blooms tied to volcanism during the 5 m.y. Permo-Triassic biotic crisis: Geology, v. 38, p. 447–450, doi:10.1130/G30769.1.

Yin, H., Zhang, K., Tong, J., Yang, Z., and Wu, S., 2001, The global stratotype section and point (GSSP) of the Permian-Triassic boundary: Episodes, v. 24, p. 102–117.

Science Editor: A. Hope Jahren
Associate Editor: Kenneth G. MacLeod

Manuscript Received 25 August 2014
Revised Manuscript Received 9 December 2014
Manuscript Accepted 24 February 2015

Printed in the USA

Geological Society of America Bulletin

Progressive environmental deterioration in northwestern Pangea leading to the latest Permian extinction

Stephen E. Grasby, Benoit Beauchamp, David P.G. Bond, Paul Wignall, Cristina Talavera, Jennifer M. Galloway, Karsten Piepjohn, Lutz Reinhardt and Dierk Blomeier

Geological Society of America Bulletin 2015;127, no. 9-10;1331-1347
doi: 10.1130/B31197.1

Notes